

THERMAL ANALYSIS OF GLASS – COVERED AMORPHOUS
METAL WIRES AND AMORPHOUS RIBBON FOR SECURITY
APPLICATIONS

BY

FABIENNE C. RASZEWSKI

A THESIS
SUBMITTED TO THE FACULTY OF

ALFRED UNIVERSITY

IN PARTIAL FULFILLMENT OF THE REQUIREMENTS
FOR THE DEGREE OF

MASTER OF SCIENCE

IN

GLASS SCIENCE

ALFRED, NEW YORK

OCTOBER, 2004

Alfred University theses are copyright protected and may be used for education or personal research only. Reproduction or distribution in part or whole is prohibited without written permission from the author.

THERMAL ANALYSIS OF GLASS – COVERED AMORPHOUS
METAL WIRES AND AMORPHOUS RIBBON FOR SECURITY
APPLICATIONS

BY

FABIENNE C. RASZEWSKI

B.S. ALFRED UNIVERSITY (2003)

SIGNATURE OF AUTHOR _____ (Signature on file)

APPROVED BY _____ (Signature on file)

ALEXIS CLARE, ADVISOR

(Signature on file)

WILLIAM LaCOURSE, ADVISORY COMMITTEE

(Signature on file)

MATTHEW HALL, ADVISORY COMMITTEE

(Signature on file)

DOREEN EDWARDS, CHAIR, ORAL THESIS DEFENSE

ACCEPTED BY _____ (Signature on file)

ALASTAIR CORMACK, DEAN,
SCHOOL OF ENGINEERING

ACKNOWLEDGEMENTS

My words of advice to graduate students is to write your acknowledgements first, when you are fresh to thesis writing and have not yet been exhausted by writing, more writing, and need not I forget *formatting...* and just when you think you're all done, formatting revisions. If you follow my path, there comes the day when you look through your thesis one last time, and just when you breathe a sigh of relief that it's finally done, you find a bright, white, blank page staring back at you. So here it goes....

I would like to thank Dr. Clare, my advisor, for giving me the opportunity of coming to graduate school, guiding me in the right directions and reassuring me that everyone has a bad day or bad week here and there. I would also like to thank Matt Hall for his helpful discussions about AMMorphous metals throughout this past year. Of course, without the material supplied by Prof. Chiriac and Howard Liebermann, this project would not have been possible.

Again I find myself at another "beginning," as I embark on the path to a PhD, and I would like to express my appreciation to all those who supported my decision and encouraged me on my way.

Table of Contents

Table of Contents	iv
List of Tables	v
List of Figures	vi
Abstract	viii
A. INTRODUCTION	1
B. LITERATURE SURVEY	3
1. Differential Scanning Calorimetry	3
2. Modulated® Differential Scanning Calorimetry	4
3. Thermogravimetric Analysis	7
4. Glass – Covered Amorphous Metal Wire	8
C. EXPERIMENTAL PROCEDURE	12
1. Sample Compositions	12
2. Differential Scanning Calorimetry	12
3. Modulated® Differential Scanning Calorimetry	15
4. Thermogravimetric Analysis	16
I. MDSC® OF GCAW AND AMORPHOUS RIBBON	17
A. Experimental Procedure	17
B. Results and Discussion	19
C. Conclusions	28
II. THERMAL ANALYSIS OF GCAW AND AMORPHOUS RIBBON	29
A. Experimental Procedure	29
B. Results and Discussion	30
1. Differential Scanning Calorimetry	30
2. Thermogravimetric Analysis	37
C. Conclusions	42
D. CONCLUSIONS	44
E. FUTURE WORK	47
REFERENCES	48

List of Tables

Table I.	Physical Dimensions of the GCAW	12
Table II.	Summary of Heat Capacities Determined by MDSC [®] and Traditional DSC	19
Table III.	MDSC [®] Heat Capacities Determined by Varying Instrumental Parameters	21
Table IV.	MDSC [®] Heat Capacities Determined by Varying Surface Contact	22
Table V.	Crystallization Temperatures for the GCAW and Amorphous Ribbon	31
Table VI.	Summary of the Heat Capacities Found by MDSC [®] for the Amorphous Ribbon and GCAW	33

List of Figures

Figure 1.	Typical DSC curve overlay for the calculation of heat capacity	14
Figure 2.	SEM image of the fracture surface of a FeSiB GCAW (1620 X)	17
Figure 3.	Comparison of the MDSC® and traditional DSC heat capacities of a silicon standard	20
Figure 4.	Comparison of the MDSC® heat capacities using various instrumental parameters of a silicon standard	20
Figure 5.	Comparison of MDSC® heat capacities of a silicon standard where the sample contact was manipulated	23
Figure 6.	Comparison of the MDSC® and traditional heat capacities of FeSiB GCAW	23
Figure 7.	Comparison of the MDSC® heat capacity curves of FeSiB wire to the MDSC® heat capacity curves of the silicon standard	25
Figure 8.	MDSC® relative heat capacities of the GCAW compared to the traditional heat capacity of the amorphous ribbon	25
Figure 9.	Comparison of the MDSC® heat capacities of the CoFeSiB GCAW with the glass cladding on and off	27
Figure 10.	Comparison of the total heat flow MDSC® curve and reversing heat flow MDSC® curve of the Curie transition of FeSiB amorphous ribbon	27
Figure 11.	DSC curve of the FeSiB GCAW denoting the two crystallization peaks	32
Figure 12.	Comparison of the Curie temperature of FeSiB ribbon found by DSC and TGA	32
Figure 13.	Isothermal study using the FeSiB GCAW at various annealing temperatures	38

List of Figures

Figure 14. Comparison of the TGA curves for the FeSiB amorphous ribbon and the GCAW with the Curie temperatures stated	38
Figure 15. Comparison of the TGA curves for amorphous and crystallized FeSiB ribbon	41
Figure 16. TGA curve of the FeSiB ribbon past the crystallization temperature denoting the onset crystallization temperatures of α -Fe and Fe ₃ B	41
Figure 17. TGA curve of FeSiB GCAW showing the Néel temperature behavior	42

ABSTRACT

The intent of this study was to thermally characterize glass – covered amorphous metal wires (GCAW) of compositions $\text{Co}_{66}\text{Fe}_4\text{Ni}_1\text{Si}_{15}\text{B}_{14}$, $\text{Co}_{68.28}\text{Fe}_{4.32}\text{Si}_{12.5}\text{B}_{15}$, and $\text{Fe}_{77.5}\text{Si}_{7.5}\text{B}_{15}$ and $\text{Fe}_{79}\text{Si}_9\text{B}_{12}$ amorphous ribbon, using differential scanning calorimetry (DSC), modulated[®] differential scanning calorimetry (MDSC[®]), and thermogravimetric analysis (TGA).

The crystallization temperature of the GCAW was found to increase with additions of Co and Ni. The Curie temperature of FeSiB ribbon was easily found by DSC, while it was not visible in GCAW, indicating that the glass cladding acts as a barrier towards the detection of the Curie transition. Generally, the heat capacities measured by traditional DSC were lower than those determined by MDSC[®]. Neither instrumental parameters nor sample contact had any significant influence on the heat capacities of a silicon wafer measured with MDSC[®]. Additions of Co and Ni to the FeSiB composition decreased the relative heat capacity of the GCAW. Unusually high heat capacities were measured for the GCAW and typical glass fiber by both MSDC and traditional DSC, while normal heat capacities were measured for the amorphous ribbon and silicon. Experimental results suggest that this anomaly may be due to a contact issue pertaining to the aspect ratio, but at the present time it is otherwise unexplained.

Both saturation magnetization and Curie temperature decreased with additions of Co and Ni. Two Curie temperatures were observed when the GCAW was heated to a temperature much greater than the crystallization temperature, the first corresponding to the amorphous metal and the second corresponding to the crystalline metal. The Néel temperature was also observed when the amorphous alloys were heated to $\sim 800^\circ\text{C}$.

A. INTRODUCTION

Amorphous metal wires and ribbons are not a new technology as they have been commercially available since the early eighties.¹ Due to their unique magnetic properties coupled with high strength, they were employed in various types of sensors, including electric current sensors, security sensors and mechanocardiogram sensors.^{2,3} Most of the sensor technology relies on the Large Barkhausen Effect (a large vertical step in the magnetic hysteresis loop), the Matteucci Effect (the generation of voltage when twisted wire is placed in an alternating magnetic field), or the Inverse Wiedemann Effect (a change in magnetic induction from applied torsion).^{4,5} Other sensors are based on the magnetostrictive behavior of the wires, which is a mechanical response to an applied magnetic field.^{6,7} The resurrection of glass – covered amorphous metal wire (GCAW) technology by Chiriac et al. opened up a new range of possible applications as a result of their small size.^{8,9} These new wires offered better magnetic properties even at the reduced size suggesting that the older technologies based on the “conventional” amorphous wires could be miniaturized. In addition, new technologies that rely on small or undetectable components, such as security devices, could be based on the GCAW.

Until now, research on the GCAW has been heavily focused on the magnetic behavior and, to a lesser extent, on the mechanical properties and behavior. The objective of this work was to use various methods of thermal analysis to further characterize three compositions of GCAW ($\text{Co}_{66}\text{Fe}_4\text{Ni}_1\text{Si}_{15}\text{B}_{14}$, $\text{Co}_{68.28}\text{Fe}_{4.32}\text{Si}_{12.5}\text{B}_{15}$, and $\text{Fe}_{77.5}\text{Si}_{7.5}\text{B}_{15}$) and one type of amorphous ribbon ($\text{Fe}_{79}\text{B}_{12}\text{Si}_9$). The change in the behavior of the GCAW due to temperature may provide insight to the operation limits of the wires and expose other features that prove to be useful in new technologies. Differential scanning calorimetry (DSC) was used to determine crystallization temperatures, as well heat capacities and Curie temperatures.

A relatively new thermal analysis technique, modulated[®] differential scanning calorimetry (MDSC[®]), was utilized to measure both heat capacity and Curie temperature, in addition to the glass transition temperature. Thermogravimetric analysis (TGA) was used to monitor the magnetic behavior of the GCAW and amorphous ribbon as a function of temperature.

B. LITERATURE SURVEY

1. Differential Scanning Calorimetry

The differential scanning calorimeter (DSC) is an instrument that monitors thermal events of a sample over a specific temperature range. Both the sample and reference materials are typically placed in aluminum (or platinum) sample pans, which are positioned on platforms within the DSC cell. One furnace supplies the heat to each of the platforms and the differential heat flow to the reference and sample is measured by thermocouples.¹⁰ It should be noted that this is a “heat flux DSC” by TA instruments, which must not be confused with the “power – compensated DSC” by Perkin – Elmer Corporation that has separate furnaces for both the sample and reference.¹¹

An exothermic reaction, such as crystallization, occurs when the sample releases energy, while an endothermic event occurs when the sample absorbs energy from the environment. Thus, during endothermic and exothermic processes, the heat flow differential will change as a function of temperature, until the event has ceased and the heat flow equilibrates between the sample and reference.

In addition to the detection of thermal events that consist of structural alterations, such as melting, glass transition and crystallization, the DSC can also detect transitions that involve little or no structural variations.¹¹ A good example of this is the Curie temperature, which is a typical lambda transformation; “lambda” refers to the shape of the heat capacity versus temperature curve. This temperature defines the point at which a ferromagnetic material (parallel magnetic moments) changes to a paramagnetic material (randomized magnetic moments). The heat capacity or heat flow change for Curie transitions is generally very small compared to a first order transformation, such as crystallization, since there are no significant structural changes.

Liebermann et al. have used DSC to determine the influence of annealing temperature on the Curie temperature in $\text{Fe}_{78}\text{Si}_9\text{B}_{13}$ amorphous ribbons.¹² The Curie temperature was found to increase from 397°C in the as-cast ribbon to 418°C in the ribbon annealed at 460°C for two hours. There was no evidence of a Curie temperature in the DSC thermal curve for samples annealed at 470°C and 480°C, as these samples were already partially crystallized. Zhukova et al. and Miguel et al. studied the relaxation processes in FINEMET® type glass-coated microwires ($\text{Fe}_{71.8}\text{Cu}_1\text{Nb}_{3.1}\text{Si}_{15}\text{B}_{9.1}$) and FINEMET® type amorphous alloys ($\text{Fe}_{73.5}\text{Cu}_1\text{Nb}_3\text{Si}_{15.5}\text{B}_7$), respectively.^{13,14} The Curie temperature was found to increase with both annealing time and temperature, which was the expected behavior. There was, however, the evolution of two Curie temperatures below the crystallization temperature in both studies when the samples were annealed at a temperature between 440°C and 540°C, which was attributed to the decomposition of the amorphous phase prior to crystallization. Changes in the Curie temperature were observed for even small structural reorganizations due to various annealing schedules, thus proving these measurements to be an effective approach to better understand the relaxation and crystallization processes in amorphous metals.

2. Modulated® Differential Scanning Calorimetry

Modulated® differential scanning calorimetry (MDSC®), a relatively recent technology, was developed by Reading et al. in the early nineties when it was found that more information could be gained from a single heat cycle if the temperature was modulated with a “sinusoidal ripple.”¹⁵ It is important to note that MDSC® is merely an extension of the traditional “heat flux DSC,” the only difference being what dictates heat flow. In traditional DSC, heat flow is based on a linear rise in temperature, given by:

$$\frac{dQ}{dt} = Cp \cdot \frac{dT}{dt} + f(t, T) \quad (1)$$

where: Q = amount of heat evolved
 Cp = heat capacity
 T = absolute temperature
 t = time
 $f(t, T)$ = some function of time and temperature that governs the kinetic response of any physical or chemical transformation

Due to the sinusoidal ripple, the temperature component of MDSC[®] is then governed by both a frequency and amplitude, which can be seen in the following equation:

$$T = bt + B \cdot \sin(\omega t) \quad (2)$$

where: ω = frequency
 b = heating rate
 B = amplitude of temperature modulation

The original heat flow equation can then be represented as:¹⁶

$$\frac{dQ}{dt} = -\frac{dT}{dt} [Cp + f'(t, T)] + f(t, T) \quad (3)$$

where: $f'(t, T)$ = thermodynamic heat flow component
 $f(t, T)$ = kinetically – limited heat flow

Thus total heat flow is influenced by both a heating rate dependent reaction and one that is only controlled by absolute temperature. A reversing

reaction, which is a transition that can be repeated throughout heating and cooling cycles, is dependent on the heating rate component. Examples of this type of transition include heat capacity and glass transition (T_g). It should be noted that the glass transition is also dependent on the frequency of modulation. Transitions, such as relaxation and evaporation, are non – reversing processes that are temperature dependent and cannot be reversed once initiated. During data collection, a discrete Fourier transformation of the total heat flow is performed, allowing the user to separate the reversing and non – reversing components.¹⁷ This proves to be extremely useful when there are overlapping reactions in a material. Another benefit of MDSC® is that it measures heat capacity directly, eliminating the need to calculate heat capacity as described in ASTM Designation: E 1269 – 99.¹⁸ The calculation of heat capacity by the instrument (also by a discrete Fourier transformation) is based on the comparison of the measured amplitude of the sample temperature and heat flow modulation to a reference sine wave of the same frequency, which can be seen in the following equation:¹⁰

$$C_p = K_{Cp} \cdot \frac{Q_{amp}}{T_{amp}} \cdot \frac{M_{per}}{2\pi} \quad (4)$$

where:

- C_p = heat capacity
- K_{Cp} = heat capacity calibration constant
- Q_{amp} = heat flow amplitude
- T_{amp} = temperature amplitude
- M_{per} = period of modulation

Recently, there have been a number of studies involving the analysis of metallic glass, also termed amorphous metal alloys, with the modulated® differential scanning calorimeter. The glass transition temperature of

metallic glasses is typically so close to the crystallization temperature that it is not detected when traditional DSC is used.

Marzo et al. studied the nanocrystallization of a FINEMET® alloy having a composition of $\text{Fe}_{73.5}\text{Si}_{13.5}\text{B}_9\text{Cu}_1\text{Nb}_3$.¹⁹ The Curie temperature of the as – cast glassy phase appeared as a small endothermic peak on the reversing curve at 315°C. The onset of crystallization was observed at 519°C as an exothermic peak on the non – reversing curve, while a slight drop in heat flow was also noticed at this temperature on the reversing curve. The unknown heat flow drop was determined to be the glass transition after they found that it shifted to higher temperatures as the modulation period was decreased. Thus by changing the frequency, a rate controlled process, such as the glass transition, can be discerned from other features on the DSC curve.

The separation of the glass transition and crystallization by MDSC® of several metallic glasses, including $\text{La}_{55}\text{Al}_{25}\text{Ni}_{20}$, $\text{Zn}_{65}\text{Mg}_{35}$, $\text{Nd}_{60}\text{Fe}_{30}\text{Al}_{10}$, and $\text{Zr}_{30}\text{Y}_{30}\text{Al}_{15}\text{Ni}_{25}$, has been studied in detail by Li et al.²⁰ The only glass transition found by traditional DSC was in $\text{La}_{55}\text{Al}_{25}\text{Ni}_{20}$ where there was a sufficient temperature separation between the T_g (196°C) and onset of crystallization (246°C). The glass transition of the other glasses was only detected by the MDSC® and could clearly be seen in the reversing heat flow curve as the drop in the heat flow. The presence of a second T_g is also noted for the $\text{Zn}_{65}\text{Mg}_{35}$ and $\text{Zr}_{30}\text{Y}_{30}\text{Al}_{15}\text{Ni}_{25}$ glasses. No other experiments, involving the use of variable frequency, were performed to verify that the “clear step change in heat flow” was actually from the glass transition. Thus it is questionable as to whether or not these metallic glasses really do possess two glass transition temperatures.

3. Thermogravimetric Analysis

Thermogravimetric analysis (TGA) is typically used to determine the amount of weight lost or gained by a material as a function of temperature. In this instrument a sample and tare platinum pan are hung from a balance

arm that is kept in the “null” position by a transducer coil that monitors current.²¹ The position of the beam is observed by an infrared light emitting diode (LED) source and a matched photodiode pair, while a flag on the balance arm controls the amount of light incident on the photodiodes. As the weight of the sample changes with temperature, an electrical current is used to maintain the balance, which is directly proportional to the weight change in the material. Another application of the TGA is to determine Curie temperatures in ferromagnetic materials, as described in ASTM Designation E: 1582 – 93, which is actually a technique for temperature calibration of the TGA.²² When the material is placed under a magnetic field, there is an apparent weight gain as the magnet pulls the sample towards it. The weight gain gradually decreases to zero percent as the ferromagnetic material becomes paramagnetic at the Curie temperature since it no longer has a permanent magnetic moment.

Luborsky et al. found this to be a suitable method for determining the Curie transition in numerous Fe – B – Si amorphous alloys.²³ The Curie temperature was found to slightly increase as silicon replaced boron and a rapid decrease in Curie temperature, as low as 221°C, was observed for high iron contents up to ~88%. In another study also involving Fe – Si – B amorphous ribbons, Leu et al. observed changes in the magnetic behavior as the material passed through its crystallization temperature by monitoring the apparent weight loss with the TGA.²⁴ The Curie temperature was also found to increase with increasing amounts of silicon, from 395.3°C for Fe_{92.4}Si_{4.8}B_{2.8} to 421.7°C for Fe_{89.5}Si_{7.4}B_{3.1}. Curie temperatures were also determined with differential scanning calorimetry and correlated well with those values found by TGA.

4. Glass – Covered Amorphous Metal Wire

A process for making glass – covered metal wire was first implemented in 1924, when very fine wires were needed for thermocouples and resistance

thermometers.²⁵ In this technique a glass tube was filled with metal, which was then heated in a tube furnace and drawn with forceps. In order for this process to work, it was necessary that the glass be chemically inert at high temperatures with the metal and soften at a temperature between the melting and boiling point of the metal. Wires with diameters as small as 1 μm were produced and were found to have “greater tensile strength than wires of ordinary size.” This technique is commonly referred to as the Taylor method, which has become the basis for the production of amorphous glass – covered wire.

A method for making glass – covered microwire was first patented by Parkhachev in 1966, which was largely based on the Taylor method.²⁶ After the glass – covered wire was drawn it was cooled both by air jet and water, which immediately crystallized the molten metal. In 1974, the first glass – coated amorphous metal wires were produced by Wiesner and Schneider, who also used the Taylor method along with a rapid quenching technique to generate the amorphous phases.²⁷ The wires of composition $\text{Fe}_{83-x}\text{P}_{17}\text{E}_x$ ($\text{E} = \text{Ga}, \text{Ge}, \text{As}; x = 2, 4, 6, 8 \text{ at}\%$) were drawn at a speed of 2 m/s and had diameters between 10 and 20 μm . Previous rapid quenching processes, such as the plasma jet, and piston and anvil techniques, only formed amorphous alloys into powders and thin foils, approximately 20 – 75 μm thick.²⁸

Masumoto et al. developed an in – rotating water quenching technique for producing amorphous wires, in which an alloy melt is “ejected” through a small quartz nozzle by argon gas into rotating water.^{1,29} The wire is actually formed inside the rotating device, which is then passed through two magnetic rollers and then wound on a spindle outside of the rotating device. They found that both Fe and Co – based alloys, specifically Fe – Si – B and Co – Si – B, were easily formed into a fine filament with an amorphous nature using this process.³⁰ Other compositions such as Fe – P – Si and Fe – C – Si did not exhibit the excellent formability found in the previously mentioned alloys.

Although next to cobalt on the periodic table, the nickel based alloys, such as $\text{Ni}_{75}\text{Si}_8\text{B}_{17}$, were found to form “spherical shots” when made by the in – rotating water quenching. Aluminum, however, was determined to increase the forming ability of this alloy so that an amorphous wire could be produced when $\text{Ni}_{74}\text{Si}_8\text{B}_{17}\text{Al}_1$ was used. Wires fabricated by this technique were sold commercially by Unitika Ltd. for their outstanding magnetic, mechanical, and chemical properties.

Another process for producing amorphous metal wires directly from the melt, termed the glass – coated melt spinning technique, which is based on the Taylor method, was used to fabricate the wires used in this study. The glass – coated melt spinning method was almost forgotten due to the effectiveness of the in – rotating water quenching method. Recently, Chiriac et al. have resurrected this technology to fully investigate the unique properties of these microwires.⁸ In this process, an induction melter is employed and as the metal drop becomes molten the glass begins to soften. A uniform speed, between 0.5 and 7 mm/min, is used to draw a capillary, which is then rapidly cooled by a water jet to maintain the amorphous nature of the metal wire. It is imperative that this process take place in a vacuum or inert atmosphere to suppress the oxidation of the metal. Both the diameter of the wire and glass thickness is controlled by the rotation speed of the receiving drum. Some important factors in this technique include: softening temperature of the glass, melting temperature of the metal, wetting characteristics of the metal on the glass, chemical reactivity of the glass and metal, and thermal expansion coefficient matching. The glass chosen for the coating is typically a Pyrex[®] – type glass (borosilicate) or fused silica since there are not many commercially available glass tubes whose composition is compatible with the process. Wires with diameters between 3 and 25 μm with glass thicknesses between 2 and 15 μm can be produced by this method, even when using alloy compositions that have lower wire forming capabilities.

Amorphous metal wires are certainly not a new technology since they have been commercially available since the mid – eighties. Magnetic sensors and transformers have been developed due to the extremely unique magnetic behavior of the wire.²⁻⁴ The amorphous wire used in these products was made by the in – rotating water quenching technique and it has recently been termed conventional wire by those involved with the glass – covered wires (GCAW) formed by the glass – coated melt spinning technique.³¹ This new type of amorphous wire can be made smaller and it has been found to have superior magnetic properties than the conventional wire, making it an ideal material for both older and new technologies based on amorphous wires.⁹ A few examples of the applications for GCAW include: magnetic tags for surveillance purposes, stress sensors for vehicle tires, biomagnetic sensors, current sensors, detection of soil movement and earthquakes, and pressure sensors.³² Many of these sensors are based on the giant magneto – impedance (GMI) effect, the large Barkhausen effect (LBE), and the magnetostrictive behavior of the wires.^{5,6,9,31}

C. EXPERIMENTAL PROCEDURE

1. Sample Compositions

Three different compositions of glass – covered amorphous metal wire (GCAW), $\text{Co}_{66}\text{Fe}_4\text{Ni}_1\text{Si}_{15}\text{B}_{14}$, $\text{Co}_{68.28}\text{Fe}_{4.32}\text{Si}_{12.5}\text{B}_{15}$, and $\text{Fe}_{77.5}\text{Si}_{7.5}\text{B}_{15}$, were obtained from the National Institute of R&D for Technical Physics in Iasi, Romania. The glass – covered amorphous wires were formed by the glass – coated melt spinning method, using a Pyrex[®] – type glass composition.⁸ The diameter of the whole wire (glass and metal wire) and the diameter of the metal core are summarized in Table I. The amorphous ribbon used in this study has a nominal composition of $\text{Fe}_{79}\text{Si}_9\text{B}_{12}$ and was made by chill block melt – spinning.³³

Table I. Physical Dimensions of the GCAW

Composition	Metallic Core Diameter (μm)	Total Diameter (μm)
$\text{Fe}_{77.5}\text{Si}_{7.5}\text{B}_{15}$	23	42
$\text{Co}_{68.28}\text{Fe}_{4.32}\text{Si}_{12.5}\text{B}_{15}$	25	39
$\text{Co}_{66}\text{Fe}_4\text{Ni}_1\text{Si}_{15}\text{B}_{14}$	24	40

2. Differential Scanning Calorimetry

Differential scanning calorimetry (DSC) was used to determine the crystallization temperature of the GCAW and the FeSiB amorphous ribbon, as well as the Curie temperature in some of the samples. The heat capacities of the FeSiB wire and ribbon were measured with traditional DSC. Indium, tin, and zinc metal standards were used to temperature calibrate the instrument. Lengths of wire were cut into approximately 5 mm pieces and between 6 – 8 mg of sample were placed in an aluminum sample pan. The amorphous ribbon was cut into an approximate 3×3 mm piece, weighing ~ 3 – 4 mg. The reference for all runs was an empty aluminum sample pan.

Nitrogen flowed at a constant 50 mL/min to purge the DSC cell during each heat cycle.

Crystallization temperatures were measured with a TA Instruments Q10 DSC using a 20 K/min heating rate from room temperature to 600°C. The onset of crystallization was then determined with the TA Universal Analysis Software. All heat capacity measurements were done on a TA Instruments Q100 DSC, using the same sample size mentioned above. The procedure listed in ASTM Designation E 1269 – 99 was used to generate the three DSC curves necessary for the heat capacity calculation, which include a baseline (empty sample pan), a standard (sapphire), and lastly the sample.¹⁸ Samples were heated from room temperature to 400°C at 20 K/min with a five minute hold at both the beginning and end of the heating cycle so that the system could establish equilibrium.

The baseline, sapphire standard, and sample curves were plotted together on one graph to calculate the heat capacity, as designated by the ASTM standard (Figure 1). Using the known values of the sapphire heat capacity also listed in the ASTM standard, which have an associated error of 0.05% in the 150 – 900 K range, the cell constant (E) was calculated for each temperature using the following formula:³⁴

$$E = \frac{b \cdot W_{st} \cdot Cp_{st}}{60 \cdot D_{st}} \quad (5)$$

where: E = calorimetric sensitivity of the DSC (ideally this equals 1)
 Cp_{st} = specific heat capacity of the sapphire standard, J(gK)⁻¹
 b = heating rate, K/min
 D_{st} = vertical displacement between the baseline and the sapphire DSC thermal curves at a given temperature, mW (Figure 1)
 W_{st} = mass of sapphire standard, mg

Heat capacities were determined for the FeSiB wire and ribbon at 76.8°C, 126.8°C, 176.8°C, 226.8°C, 276.8°C, and 326.8°C. The cell constant, E , was then used to calculate the heat capacity of the sample (C_{p_s}) using the following equation:

$$C_{p_s} = \frac{60 \cdot E \cdot D_s}{W_s \cdot b} \quad (6)$$

where: C_{p_s} = specific heat capacity of the specimen, $J(gK)^{-1}$

D_s = vertical displacement between the baseline and the sample DSC thermal curve, mW (Figure 1)

W_s = mass of sample, mg

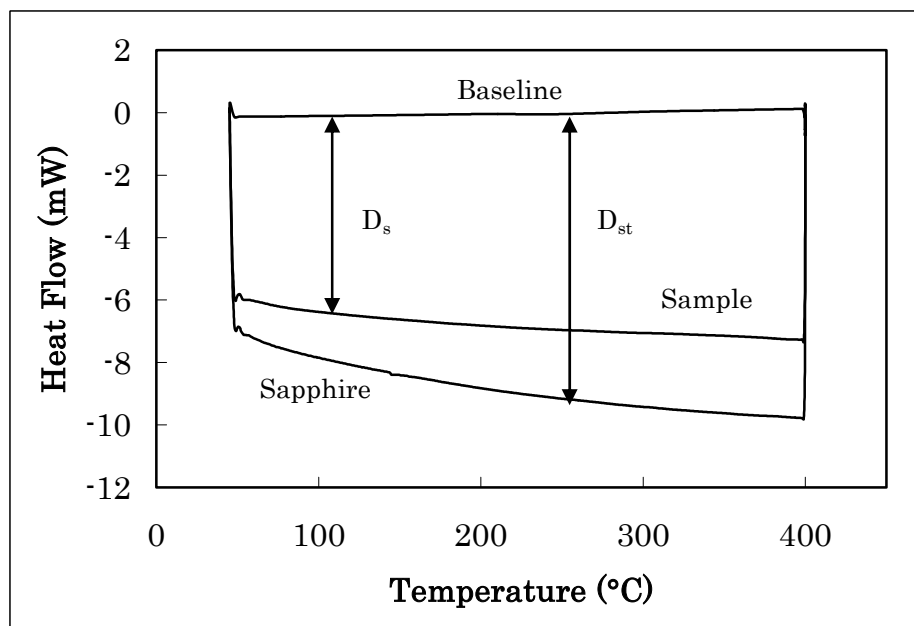


Figure 1. Typical DSC curve overlay for the calculation of heat capacity.

Isothermal experiments were carried out using the TA Instruments Q10 DSC. Samples were heated to various temperatures at or below the crystallization temperature and held for an amount of time to allow

crystallization to occur. The temperature was calibrated using the melting temperatures of In, Zn, and Sn metal standards. Between 6 – 8 mg of ~5 mm pieces of GCAW were placed into an aluminum sample pan and an empty aluminum pan was used as the reference for all heat cycles. Flowing nitrogen at 50 mL/min was used to purge the DSC cell.

3. Modulated® Differential Scanning Calorimetry

Modulated differential scanning calorimetry (MDSC®) has been used to determine the glass transition temperatures and heat capacities of all three compositions of wire and the amorphous ribbon. All measurements were performed on a TA Instruments Q100 DSC. A sapphire standard was used to calibrate the heat capacity constant of the instrument and metal standards of indium, tin and zinc were used to calibrate temperature. Between 6 – 8 mg of ~5 mm pieces of GCAW and an approximate 3 × 3 mm piece of amorphous ribbon weighing 3 – 4 mg were placed in an aluminum sample pan. An empty aluminum sample pan was used as the reference. Depending on the objective of the experiment, a 1 K/min, 3 K/min or 5 K/min heating rate was used. Since modulation is dependent on frequency, both a period and amplitude must be chosen for a conventional MDSC® heat cycle. Typical periods used in this study were 60 s, 80 s, and 100 s, with amplitudes ranging from 0.5°C to 3°C, once again depending on the objectives of the experiment. The “default” MDSC® parameters mentioned throughout this work consist of a 5°C/min heating rate, with a 1.000°C amplitude and 80 s period. Samples were only heated to 400°C due to instrumental constraints. Nitrogen flowing at 50 mL/min was used to purge the cell. In some cases the glass coating was removed from the amorphous wires using a liquid nitrogen technique developed by the author. The wires were put into a crucible filled with liquid nitrogen and were allowed to sit for at most five minutes, refilling the crucible when needed. Once the crucible warmed to room temperature,

acetone was used to rinse the wires onto a piece of paper where they were left to air dry.

Although no standard is needed for modulated[®] DSC heat capacity measurements, a silicon standard was used as a comparison throughout the study. In this case the sample size was again between 6 – 8 mg with all other instrumental parameters kept the same. The physical form of the standard, however, was altered on some occasions, either fractured into small pieces or ground into a powder with a mortar and pestle.

4. Thermogravimetric Analysis

Thermogravimetric analysis (TGA) was used to determine the magnetic the Curie temperature. A TA Instruments Q50 TGA was used for all of these measurements. Approximately 1 mg of ~5 mm pieces of GCAW were placed in a platinum sample pan for each heat cycles. An empty sample pan was used as a reference for all heat cycles. All samples were heated to 500°C at 20 K/min. Certain samples were heated beyond this temperature (as high as 800°C) to determine the magnetic behavior above the crystallization temperature. At 60°C a magnet, provided by TA Instruments, was placed underneath the TGA furnace until the end of the heat cycle, so that the magnetic behavior could be observed. Flowing nitrogen at a rate of 60 mL/min was used to purge the sample chamber, while 40 mL/min was used to purge the balance.

I. MODULATED® DIFFERENTIAL SCANNING CALORIMETRY OF GLASS – COVERED AMORPHOUS METAL WIRES AND AMORPHOUS RIBBON

A. Experimental Procedure

The glass – covered amorphous metal wires used in this study, which include $\text{Co}_{66}\text{Fe}_4\text{Ni}_1\text{Si}_{15}\text{B}_{14}$, $\text{Co}_{68.28}\text{Fe}_{4.32}\text{Si}_{12.5}\text{B}_{15}$, and $\text{Fe}_{77.5}\text{Si}_{7.5}\text{B}_{15}$, were obtained from the National Institute of Research and Development for Technical Physics in Iasi, Romania. They are approximately 40 μm in total diameter with a metallic core of $\sim 23 \mu\text{m}$ and were formed by the glass – coated melt spinning method, which is based on the Taylor method.^{8,25} A scanning electron microscopy (SEM) image of the FeSiB wire can be seen in Figure 2, in which the metallic core and glass cladding can clearly be distinguished. It should be noted that the image is misleading as to the shape of the wire due to the angle of image capture. Several other images taken at different angles clearly show the circular shape of the wires. The amorphous ribbon was formed by chill block melt – spinning and has a nominal composition of $\text{Fe}_{79}\text{B}_{12}\text{Si}_9$.³³

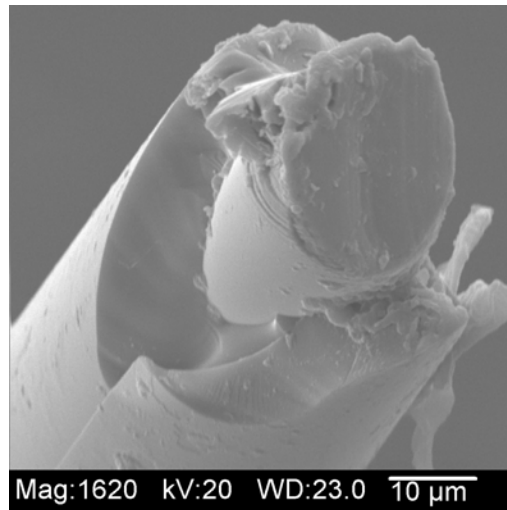


Figure 2. SEM image of the fracture surface of a FeSiB GCAW (1620 X).

The heat capacities of the FeSiB wire and ribbon, as well as a silicon standard, were determined with a TA Instruments Q100 DSC using the procedure stated in ASTM Designation: E 1269 – 99.¹⁸ A temperature calibration was performed using the melting temperatures of In, Sn, and Zn metal standards. Three heating curves, which included a baseline, sapphire standard, and sample curve, were generated for each heat capacity calculation using 20 K/min up to 400°C under a constant N₂ purge at 50 mL/min.

Heat capacities of all three glass – covered amorphous metal wires and amorphous ribbon were also determined with modulated[®] differential scanning calorimetry (MDSC[®]) using a TA Instruments Q100 DSC. In addition to the temperature calibration mentioned previously, a separate heat capacity calibration was completed using a sapphire standard. The “default” instrumental parameters used were a 5 K/min heating rate up to 400°C with a 1.000°C amplitude and an 80 s period. A constant N₂ sample purge at 50 mL/min was used to clear the DSC cell during each heat cycle. In some cases, the glass covering was removed by placing the wires in liquid nitrogen for at most 5 minutes, replenishing the liquid nitrogen when necessary. When the crucible warmed to room temperature, acetone was used to rinse the wires onto a piece of paper where they were left to air dry. The heat capacity of the silicon standard was also determined using MDSC[®]. To verify the influence of the instrumental parameters on heat capacity, one of the “default” parameters was changed for each heat cycle while the other two parameters were held constant. These other parameters include either a 1 K/min or 3 K/min heating rate, 0.5°C or 3.0°C amplitude, and a 60 s or 100 s period. Curie temperatures were also determined with MDSC[®] using the “default” parameters. Heat capacities of the silicon were also determined after altering the sample contact with the pan using the “default” instrumental parameters mentioned above. The silicon wafer was either crushed into small pieces or ground into a powder.

Images of the fracture surface of the glass – covered amorphous metal wire were taken using a Philips 515 SEM in secondary electron (SE) mode at 20 KeV with a 100 nm spot size.

B. Results and Discussion

The MDSC[®] and traditional DSC heat capacity results for a semiconductor grade silicon wafer can be seen in Figure 3 and are listed in Table II. Heat capacities obtained by the traditional DSC method are somewhat lower than those measured by MDSC[®], but the MDSC[®] values are closer to the literature values. The reported literature values of heat capacity, however, are still within the experimental error for both techniques.³⁵

Table II. Summary of Heat Capacities Determined by MDSC[®] and Traditional DSC

Temperature (°C)	Heat Capacity J(gK) ⁻¹		
	Traditional DSC	Modulated [®] DSC	Literature
76.85	0.73 ± 0.03	0.74 ± 0.03	0.7577
126.85	0.76 ± 0.03	0.78 ± 0.04	0.7883
226.85	0.80 ± 0.04	0.84 ± 0.03	0.8307
326.85	0.83 ± 0.06	0.87 ± 0.02	0.8599

To understand the nature of the differences between MDSC[®] and traditional DSC, the experimental parameters were varied. The influence of the instrumental parameters can be seen in Figure 4 and Table III. In general, the heat capacities found by changing the period and amplitude from the default conditions were lower than the literature values, while those heat capacities generated with the 1 K/min and 3 K/min heating rate were higher. The “default” instrumental parameters yielded the best heat capacity results and were therefore used to measure all other heat capacities in the study.

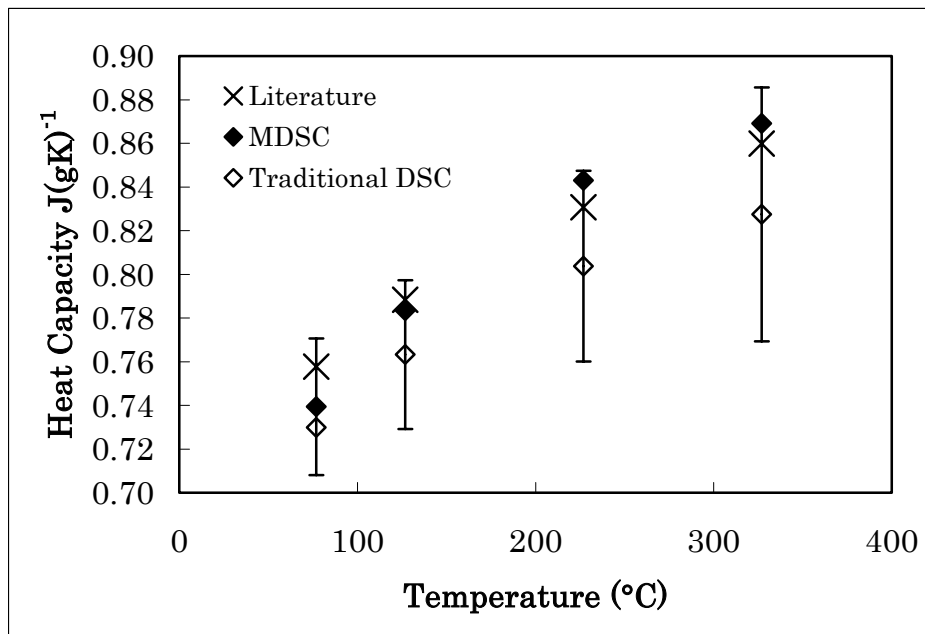


Figure 3. Comparison of the MDSC[®] and traditional DSC heat capacities of a silicon standard. Note: MDSC[®] error bars remain relatively constant throughout temperature range.

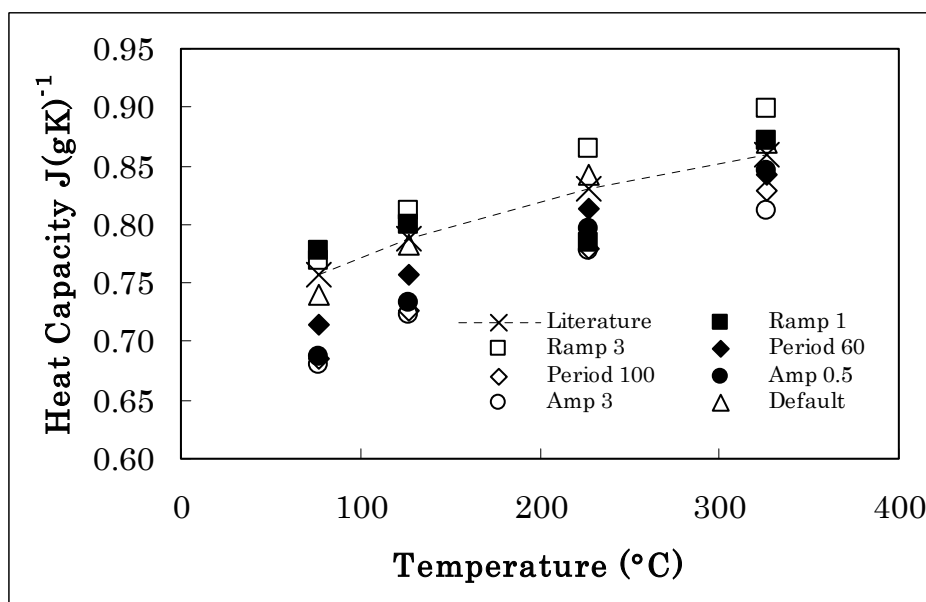


Figure 4. Comparison of the MDSC[®] heat capacities using various instrumental parameters of a silicon standard. Error bars are not shown for clarity.

Sample geometry and therefore contact with the sample pan also had an effect. The best results were obtained with the whole piece, followed by crushed pieces, and then powder, when compared to the literature values, as seen in Figure 5 and Table IV. The single piece of silicon had the most ideal contact in that there was less room for air between the sample and the pan, thus yielding the best results. When the sample was crushed into smaller pieces and powder, the contact was less optimal and the heat capacities deviated more from the literature values. Again, the reported literature values were within the instrumental error for all three types of samples.

Table III. MDSC® Heat Capacities Determined by Varying Instrumental Parameters

Temperature (°C)	Heat Capacity J(gK) ⁻¹			
	Literature	Default	Ramp Rate 1 K/min	Ramp Rate 3 K/min
76.85	0.7577	0.74 ± 0.03	0.78 ± 0.01	0.77 ± 0.002
126.85	0.7883	0.78 ± 0.03	0.80 ± 0.01	0.81 ± 0.005
226.85	0.8307	0.84 ± 0.03	0.78 ± 0.007	0.86 ± 0.002
326.85	0.8599	0.87 ± 0.02	0.87 ± 0.03	0.90 ± 0.03

Temperature (°C)	Period	Period	Amplitude	Amplitude
	60 s	100 s	0.5°C	3.0°C
76.85	0.71 ± 0.05	0.69 ± 0.004	0.69 ± 0.001	0.68 ± 0.005
126.85	0.76 ± 0.04	0.73 ± 0.005	0.73 ± 0.002	0.72 ± 0.003
226.85	0.81 ± 0.05	0.78 ± 0.002	0.80 ± 0.005	0.78 ± 0.01
326.85	0.84 ± 0.05	0.83 ± 0.01	0.85 ± 0.004	0.81 ± 0.01

Table IV. MDSC[®] Heat Capacities Determined by Varying Surface Contact

Temperature (°C)	Heat Capacity J(gK) ⁻¹		
	Whole Piece	Pieces	Powder
76.85	0.73 ± 0.04	0.70 ± 0.07	0.68 ± 0.07
126.85	0.77 ± 0.04	0.75 ± 0.07	0.72 ± 0.07
226.85	0.82 ± 0.03	0.82 ± 0.08	0.79 ± 0.06
326.85	0.87 ± 0.02	0.93 ± 0.09	0.88 ± 0.04

Both traditional DSC and MDSC[®] were performed on the same FeSiB GCAW, the results of which can be seen in Figure 6. In six heat cycles on the same wire, there was almost no variation in the heat capacities determined by MDSC[®], however, a spread was present for heat capacities determined by traditional DSC. It should be noted that the spread was not systematic. Since heat capacity can be measured directly by MDSC[®] there is no need to move the sample after each run or open the DSC cell. In the traditional DSC, three curves are necessary for the calculation of heat capacity, so there is repeated movement within the cell between each heat cycle, altering both cell atmosphere and pan position on the platform. These changes may account for some differences in heat capacity found by traditional DSC and it therefore appears that MDSC[®] is a more efficient and consistent method for measuring heat capacity.

The modulated[®] DSC results are again higher than those found by traditional DSC. The heat capacity results are also repeatable up to as many as 10 thermal cycles, indicating that there is not enough energy stored in the wires due to the forming method to substantially alter the heat capacity after repeated heat treatments. If there was excess energy, the heat capacity would have changed due to the structural relaxation in the material during the repeated heat cycles.

Throughout the course of the study it was noticed that there was a significant variation in the heat capacities of the FeSiB wire as more wire

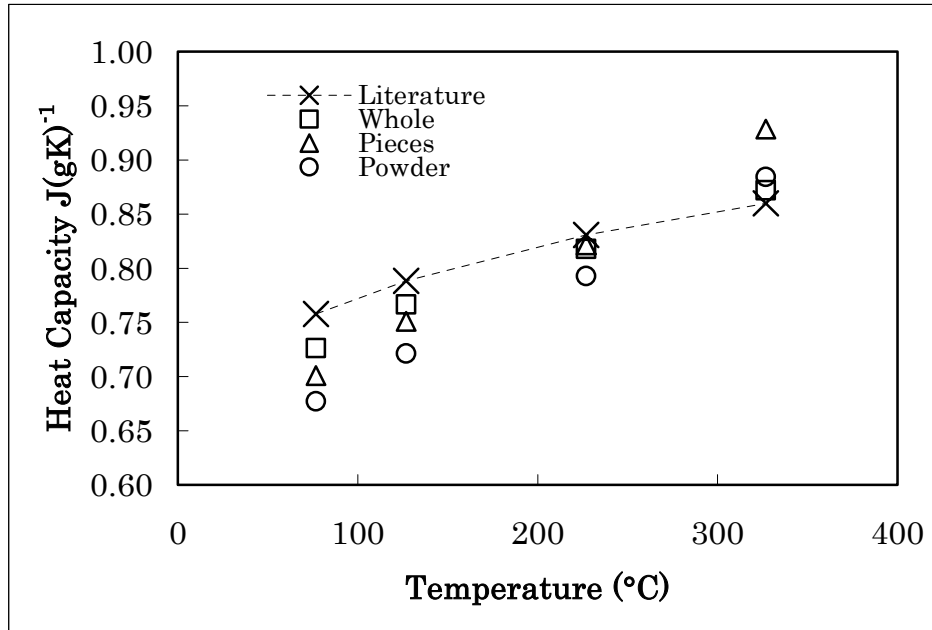


Figure 5. Comparison of MDSC® heat capacities of a silicon standard where the sample contact was manipulated. Error bars are not shown for clarity.

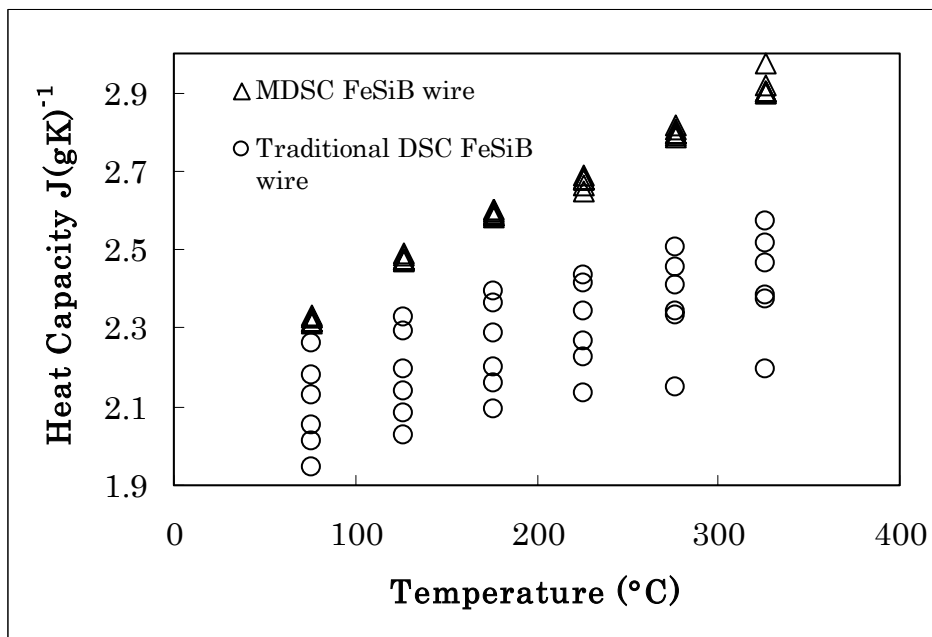


Figure 6. Comparison of the MDSC® and traditional heat capacities of FeSiB GCAW.

was consumed and tested. The spread is even more prominent when the FeSiB and silicon heat capacities are plotted together as seen in Figure 7. Non – uniform cooling could induce different fictive structures along the length of the wire, therefore producing noticeable disparities in heat capacity. In addition, deviations in glass thickness may also influence the heat capacity of the wire, but this would most likely be a small effect compared to the influence of structure.

Compared to silicon, the measured heat capacity of the FeSiB wire is much higher on a per gram basis, $\sim 0.7 \text{ J(gK)}^{-1}$ for silicon versus $\sim 2 \text{ J(gK)}^{-1}$ for the GCAW at 76.85°C . When calculated on a mole basis, the measured heat capacity of FeSiB wire is 13 times the value of R (8.314 J(gK)^{-1}) at 76.85°C , which approaches $\sim 22R$ at 326.85°C . This is theoretically impossible since lattice heat capacities of all solids reach a maximum value of $3R$, where $R = 8.314 \text{ J (mol K)}^{-1}$, at high temperatures.³⁶

The same anomaly was also observed in the heat capacity results for the CoFeSiB and CoFeNiSiB wires as seen in Figure 8. The heat capacities of these GCAW are somewhat lower than those in the FeSiB wire due to differences in electronic heat capacity contribution and thermal expansion, but both are still much greater than the $3R$ limit. This behavior is seen in the heat capacities determined by traditional DSC as well, although the discrepancy is not as high (Figure 6). The traditional DSC heat capacity results of the FeSiB amorphous ribbon are compared to the MDSC[®] heat capacities of the GCAW in Figure 8. The amorphous ribbon heat capacities are much lower and are below the $3R$ limit, indicating that the anomalous heat capacity in the wires is likely due to their size and contact. Glass removal further increased the heat capacity of all three of the wires, which can be seen in Figure 9. To be certain that this behavior was not only present in GCAW, MDSC[®] was also used to determine the heat capacity of typical borosilicate glass fiber with the fiber diameter being much less than the diameter of the GCAW. The heat capacity of the glass fiber was

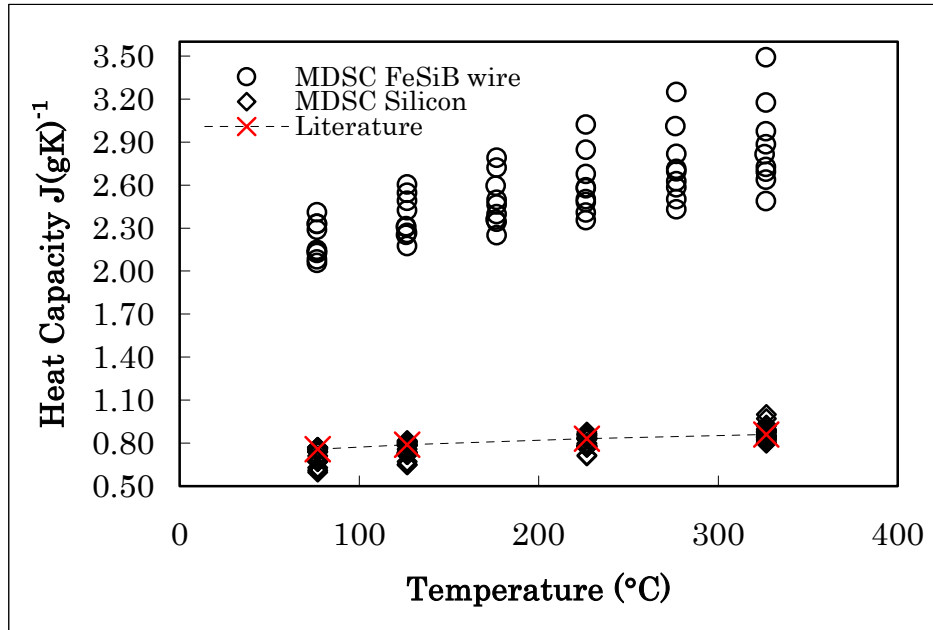


Figure 7. Comparison of the MDSC[®] heat capacity curves of FeSiB wire to the MDSC[®] heat capacity curves of the silicon standard.

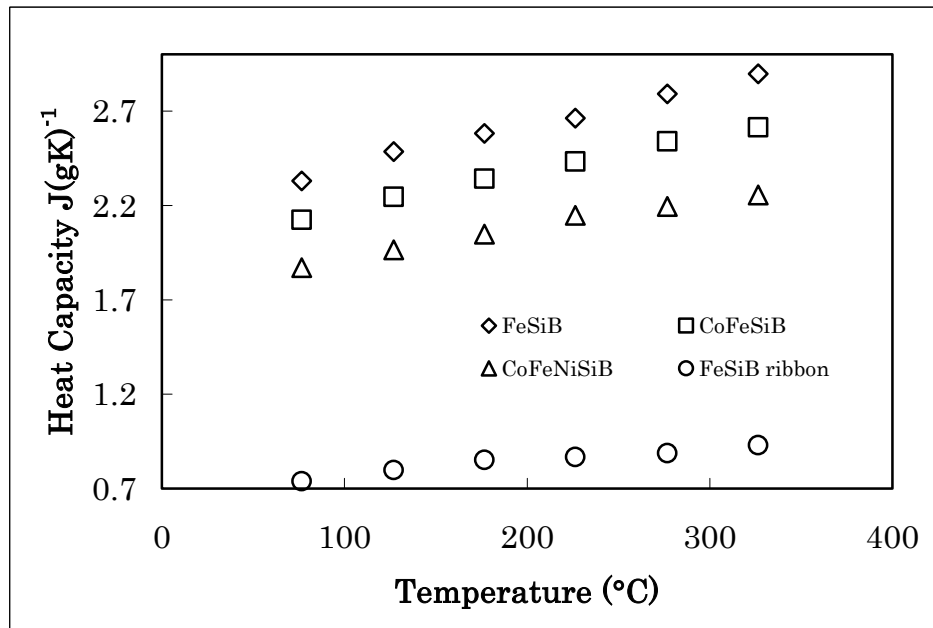


Figure 8. MDSC[®] relative heat capacities of the GCAW compared to the traditional heat capacity of the amorphous ribbon.

even higher than the heat capacity of the FeSiB wire ($\sim 3 \text{ J(gK)}^{-1}$ at 76.85°C), proving this to be an anomaly in the heat capacity measurement of fiber – like geometries. The measured heat capacity appears to increase with a corresponding decrease in fiber diameter, as this was demonstrated when the glass was removed, as well as when very small diameter glass fiber was measured. When the glass fiber was ground into a powder, the heat capacity was significantly decreased to values well below the 3R limit. The heat capacity of the FeSiB wire was reduced when placed in alumina powder, which suggests that the anomaly is a contact issue since the presence of the alumina powder would promote enhanced heat flow. At the present time the exact origin of the anomaly is unknown, however, there is experimental evidence that indicates the unexpected behavior to be due to contact of fiber – like geometries. It is possible that in the same way that fiberglass insulation is an effective thermal barrier; the presence of the high aspect ratio fiber blocks the heat transfer in the sample pan. The reason for the consistently high heat capacities measured by MDSC[®] is not known.

The Curie temperature of the FeSiB amorphous metal ribbon, which occurs at 389°C , was also found using MDSC[®], as seen in Figure 10. This correlates well with the Curie temperatures found by traditional DSC and TGA. A very small change in heat capacity ($\leq 0.1 \text{ J(gK)}^{-1}$) is associated with this transition and in some cases it is lost in the background of a traditional DSC curve.¹¹ Since MDSC[®] is quite sensitive and able to separate reversing and non – reversing reactions from the total heat flow, the Curie transition can be clearly observed on both the total heat flow curve and reversing heat flow curve. Marzo et al. also used MDSC[®] to determine the Curie temperature a FINEMET[®] type alloy of composition $\text{Fe}_{73.5}\text{Si}_{13.5}\text{B}_9\text{Cu}_1\text{Nb}_3$.¹⁹ The transition was quite clear on the reversing heat flow curve and looked very similar to the one found in this study.

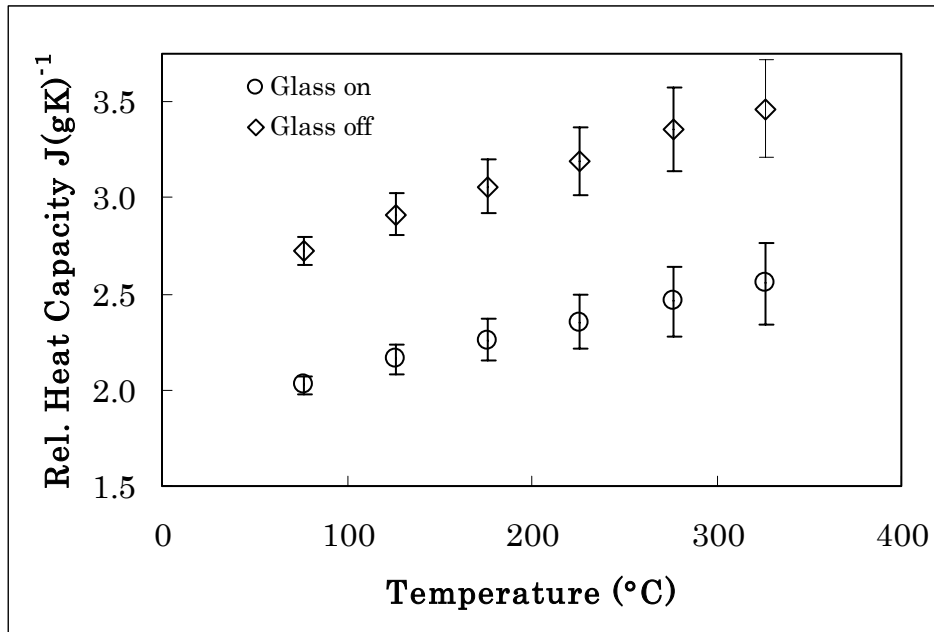


Figure 9. Comparison of the MDSC[®] heat capacities of the CoFeSiB GCAW with the glass cladding on and off.

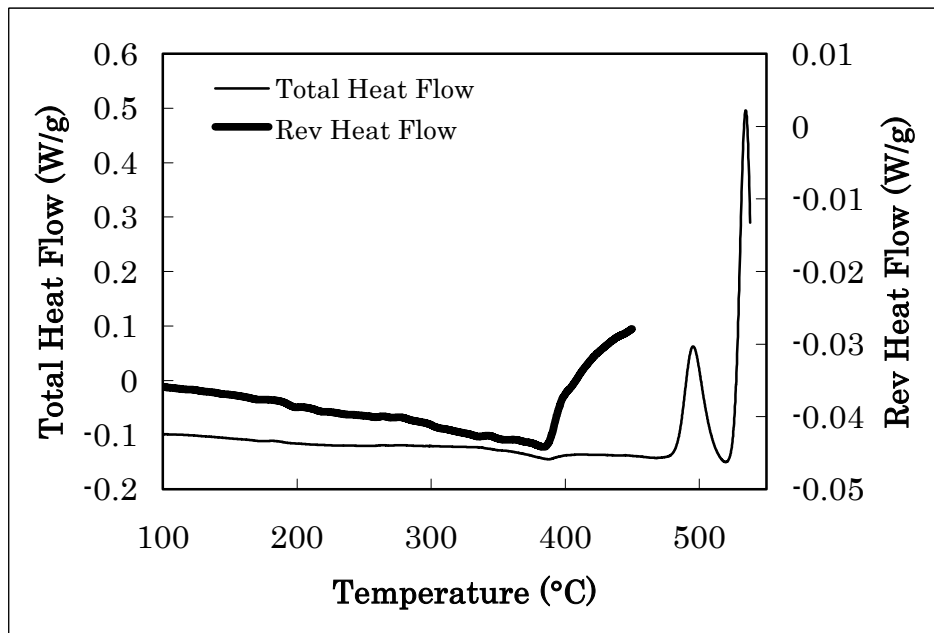


Figure 10. Comparison of the total heat flow MDSC[®] curve and reversing heat flow MDSC[®] curve of the Curie transition of FeSiB amorphous ribbon.

C. Conclusions

MDSC[®] has been shown to be an efficient and consistent method for measuring heat capacity, compared to the traditional DSC technique, provided an appropriate sample geometry is chosen. Altering instrumental parameters, including heating rate, period, and amplitude, or sample surface area did not have any adverse effects on the measured heat capacities of a silicon standard. The heat capacities of the FeSiB wire show little variation even after being subjected to 10 thermal cycles up to 400°C, indicating that very little relaxation takes place within the wire. A spread in the heat capacities of the various FeSiB wire sections heat capacities was observed which may be due to structural differences along the length of wire. The measured heat capacities of all three wires exceeded the 3R maximum, while the heat capacity of the FeSiB amorphous ribbon stayed well below this limit throughout the entire temperature range. Anomalous heat capacities were also measured for typical borosilicate glass fiber and GCAW without the glass cladding. Heat capacities of the glass fiber were lowered (<3R) when it was ground into a powder. Lower heat capacities were also observed for the FeSiB wire, when placed in alumina powder, suggesting an anomaly exists in the heat capacity measurement of fiber – like geometries. The exact origin of the unexpected behavior is otherwise unknown at this time. The Curie temperature of the FeSiB amorphous ribbon was also found using MDSC[®] at 389°C and, since it is a reversing reaction, it can clearly be observed on the total heat flow and reversing heat flow curves.

II. THERMAL ANALYSIS OF GLASS – COVERED AMORPHOUS METAL WIRE AND AMORPHOUS RIBBON

A. Experimental Procedure

The glass covered amorphous metal wires formed by the glass – coated melt spinning method were obtained from the National Institute of Research and Development for Technical Physics in Iasi, Romania.^{8,25} Three compositions were characterized, which include $\text{Co}_{66}\text{Fe}_4\text{Ni}_1\text{Si}_{15}\text{B}_{14}$, $\text{Co}_{68.28}\text{Fe}_{4.32}\text{Si}_{12.5}\text{B}_{15}$, and $\text{Fe}_{77.5}\text{Si}_{7.5}\text{B}_{15}$. The amorphous metal ribbon has a nominal composition of $\text{Fe}_{79}\text{B}_{12}\text{Si}_9$ and was formed by chill block melt – spinning.³³

Crystallization temperatures of the GCAW were determined with a TA Instruments DSC Q10 Differential Scanning Calorimeter. The samples were heated to 600°C at a rate of 20 K/min with a constant N_2 sample purge. A temperature calibration was performed by using the melting temperatures of In, Sn, and Zn standards.

The three heating curves necessary for heat capacity calculation, as stated in ASTM Designation: E 1269 – 99, were made using a TA Instruments DSC Q100 Differential Scanning Calorimeter. The wires were heated to 400°C at 20 K/min with a constant N_2 sample purge. Additional heat capacity measurements were made using modulated[®] differential scanning calorimetry (MDSC[®]), which is an extension of the conventional Q100 DSC by TA Instruments. The GCAW were heated to 400°C at 5 K/min with an 80 s period and 1.0°C amplitude. No further calculations were necessary as heat capacity is directly determined by the instrument. A temperature calibration was performed using the melting temperatures of the In, Sn and Zn metal standards. An additional heat capacity calibration for the modulated[®] DSC was also completed using a sapphire standard. For

those experiments involving only the bare wire, glass removal was accomplished by putting the glass – covered wires in liquid nitrogen. The wires are first cut into approximately 3 mm pieces and then placed in a dish containing liquid nitrogen, which is replenished approximately three times. Acetone was used to rinse the wires out of the dish and onto a piece of paper where the wires can be collected. An attempt to find the glass transition was also performed using the MDSC[®] with similar experimental parameters listed above, except for an upper temperature of 550°C.

Isothermal experiments were performed using the TA Instruments Q10 DSC. Samples were heated to various temperatures and held until crystallization was completed. Some samples were heated to temperature at 20 K/min after the isothermal hold. Flowing nitrogen at 50 mL/min was used to purge the DSC cell during each heat cycle. The temperature was calibrated using the melting temperatures of In, Zn, and Sn metal standards.

Curie temperatures were determined with a TA Instruments Q50 TGA. Samples were heated to the peak temperature at 20K/min with a constant N₂ purge. At 60°C a bar magnet, supplied by TA Instruments, was placed under the furnace to allow heating under a magnetic field, allowing demagnetization to be observed as weight loss.

B. Results and Discussion

1. Differential Scanning Calorimetry

The crystallization temperatures (T_x) of the CoFeNiSiB can be seen in Table V. It should be noted that the FeSiB wire and ribbon possess two overlapping crystallization peaks, as seen in Figure 11. The first peak corresponds to the crystallization of α – (Fe, Si) while the second peak corresponds to the boride phase, Fe₃B.¹² Bang and Lee performed a crystallization study on Fe₇₈B₁₃Si₉ amorphous ribbon, which is very similar in composition to the GCAW and ribbon used in this study.³⁷ When the sample

was heat treated at 450°C for 1 hour, two different crystal structures were found to evolve (verified by XRD); solid solution $\alpha - (\text{Fe},\text{Si})$ and metastable Fe_3B . After heat treatment at 550°C for 1 hour, the metastable Fe_3B decomposed into stable Fe_2B and $\alpha - (\text{Fe},\text{Si})$.

Table V. Crystallization Temperatures for the GCAW and Amorphous Ribbon

Composition	T_x (°C)
$\text{Fe}_{79}\text{Si}_9\text{B}_{12}$ ribbon	502, 549
$\text{Fe}_{77.5}\text{Si}_{7.5}\text{B}_{15}$	541, 556
$\text{Co}_{68.28}\text{Fe}_{4.32}\text{Si}_{12.5}\text{B}_{15}$	546
$\text{Co}_{66}\text{Fe}_4\text{Ni}_1\text{Si}_{15}\text{B}_{14}$	559

The addition of Co and Ni increase the onset of crystallization approximately 20°C above that of the FeSiB GCAW. These atoms inhibit atomic movement raising the kinetic barrier for crystallization. The crystallization temperatures of the FeSiB ribbon were slightly lower than for the FeSiB wire. This may be due to composition, as there are slightly different amounts of Si and B in the two materials. Surface crystallization may be another cause, but since glass removal does not cause any shift in the crystallization onset temperatures for any of the wires, it is doubtful that this would cause the difference. Lastly, nuclei may be present in the ribbon that are absent in the wires permitting crystallization at a lower temperature.

An interesting aspect of the DSC curve for the FeSiB ribbon is that the Curie temperature is discernable (Figure 12). It is represented by a small change in heat capacity at 389°C, the classic lambda transition, which is approximately $0.1 \text{ J}(\text{gK})^{-1}$. An endothermic reaction occurs just below the Curie temperature as energy is being absorbed by the sample to induce randomization of the magnetic dipoles.¹¹ An exothermic event occurs directly after the Curie temperature since no further energy is needed for randomization. This transition is not found in the DSC curves for any of the

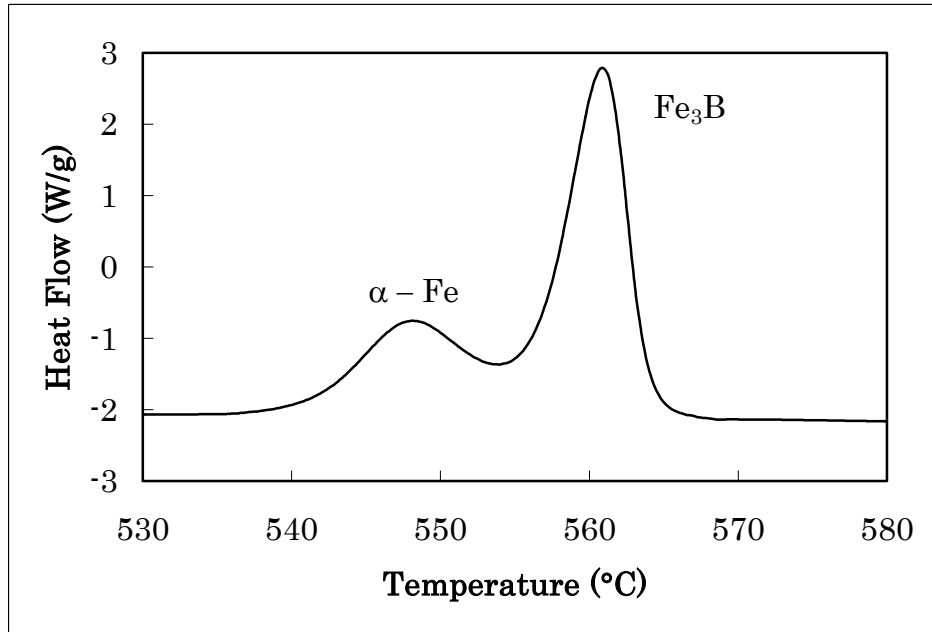


Figure 11. DSC curve of the FeSiB GCAW denoting the two crystallization peaks.

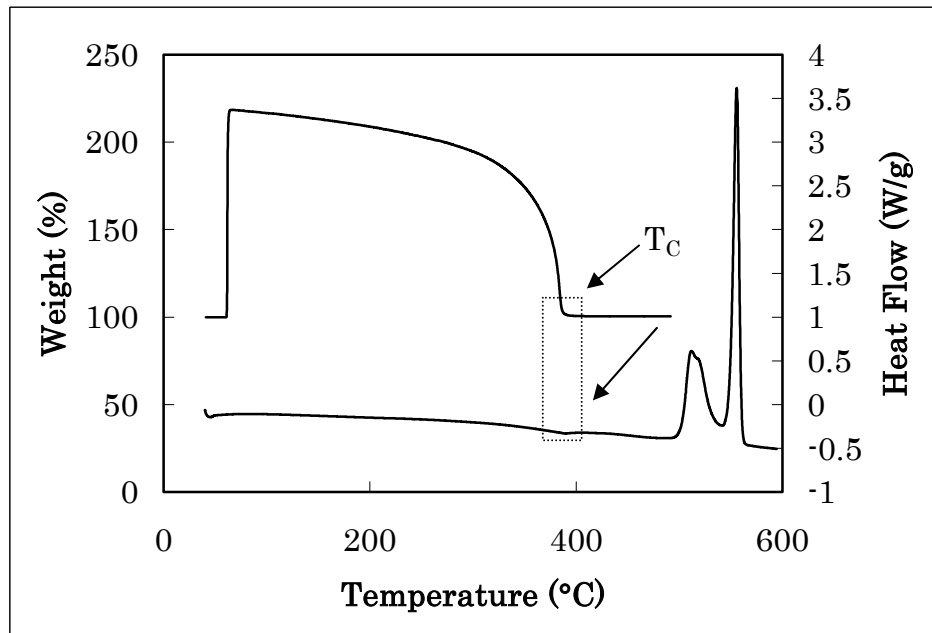


Figure 12. Comparison of the Curie temperature of FeSiB ribbon found by DSC and TGA. Note: TGA measurement was taken under the influence of a magnetic field.

glass – covered amorphous metal wires. If the glass covering is removed, however, the Curie transition is visible in the FeSiB wire. DSC detects the Curie temperature as a change in heat flow and due to the small amount of energy associated with this transition, it is not perceived when the glass is present. When the glass is removed, however, and the metal wire is in direct contact with the sample pan, there is sufficient heat flow for the Curie transition to be detected.

Heat capacities were measured by traditional DSC for the FeSiB wire and ribbon from 76°C to 326°C at 50°C intervals and are listed in Table VI. These were used as a comparison for heat capacities measured by MDSC®. The heat capacities of each wire composition found by modulated® DSC are also listed in Table VI.

Table VI. Summary of the Heat Capacities Found by MDSC® for the Amorphous Ribbon and GCAW

	Heat Capacity J(gK) ⁻¹					
	76.85°C	126.85°C	176.85°C	226.85°C	276.85°C	326.85°C
FeSiB ribbon*	0.74 ± 0.03	0.80 ± 0.04	0.85 ± 0.04	0.87 ± 0.05	0.89 ± 0.05	0.93 ± 0.04
FeSiB wire*	2.10 ± 0.12	2.18 ± 0.12	2.25 ± 0.12	2.30 ± 0.12	2.37 ± 0.13	2.42 ± 0.13
FeSiB wire	2.32 ± 0.01	2.48 ± 0.01	2.59 ± 0.01	2.67 ± 0.01	2.80 ± 0.01	2.92 ± 0.01
CoFeSiB wire	2.18 ± 0.04	2.30 ± 0.06	2.39 ± 0.07	2.48 ± 0.08	2.58 ± 0.09	2.64 ± 0.11
CoFeNiSiB wire	1.87 ± 0.01	1.96 ± 0.01	2.05 ± 0.02	2.12 ± 0.03	2.15 ± 0.04	2.20 ± 0.05

Note: A (*) denotes those heat capacities determined by traditional DSC

Six successive runs were completed on the same FeSiB sample with both the traditional and MDSC®. The range of heat capacities found by traditional DSC is quite large, while those determined by MDSC® were relatively constant (Figure 6). The influence of experimental parameters (heating rate, period, and amplitude) on heat capacity of the same FeSiB sample was also investigated using the MDSC®. One parameter was altered during each measurement from the default parameter of a 5 K/min heating rate with an 80 s period and 1.0°C amplitude. These variations included a 0.5°C and

3.0°C amplitude, a 1 K/min and 3 K/min heat rate, and a 60 s and 100 s period. It was found that heat capacity is insensitive to the experimental parameters within experimental error.

Modulated[®] DSC was used to determine the heat capacities for the CoFeSiB and CoFeNiSiB wire, as it was demonstrated to be an accurate and efficient method to find heat capacities of the amorphous wires. It is evident that as Co and Ni are added to FeSiB the heat capacity decreases, which may be due to the influence of the electronic heat capacity on the total heat capacity; increasing the number of free electrons per unit volume will increase the contribution of the electronic heat capacity, thus raising the total heat capacity.³⁸ Large differences in the phonon heat capacity are not expected at these temperatures. The electronic heat capacity (C_e) for the FeSiB ribbon was determined to be $0.05 \text{ J}(\text{mol K})^{-1}$ at 76.8°C from the following two equations:³⁹

$$E_F = \left(\frac{h^2}{2m} \right) \left(\frac{3N}{8\pi} \right)^{\frac{2}{3}} \quad (7)$$

where: E_F = Fermi energy
 h = Planck's constant ($6.626 \times 10^{-34} \text{ kg} \cdot \text{m}^2 \cdot \text{s}^{-1}$)
 m = molecular weight
 N = # of electrons/volume

$$C_{el} = \left(\frac{2N_A k^2}{E_F} T \right) \quad (8)$$

where: N_A = Avogadro's number (6.022×10^{23} atoms/mole)
 k = Boltzmann's constant ($1.38 \times 10^{-23} \text{ J/K}$)
 T = temperature

The Fermi energy calculation was based on two assumptions; the ribbon had a density of 7.1 g/cm^3 and the iron provided 2 free electrons while the silicon and boron provided none. By itself, iron has a Fermi energy of 11.1 eV, which is reduced to 9.2 eV in the amorphous ribbon, indicating that the presence of boron and silicon decrease this energy.³⁸ Compared to the measured heat capacity of $38.7 \text{ J(mol K)}^{-1}$ at 76.8°C , the electronic heat capacity has a relatively small contribution. It is probable that the differences in electronic heat capacity of the GCAW are due to differences in density, which would influence the number of free electrons per unit volume. At this time, however, the densities of the GCAW are unknown and no further calculations could be made.

Interestingly, when comparing the heat capacity of the FeSiB ribbon to the wire, the values seem abnormally high for all three of the wires as seen in Figure 8. Investigation of this phenomenon revealed it to be a function of the aspect ratio of the wire. An experiment on silicon demonstrated that a powder or a bulk sample did not change the measured heat capacity beyond experimental error. In fact, the powdered samples rendered lower heat capacities than the bulk. This anomaly was found to occur in typical oxide glass fiber as well. Samples of the glass fiber yielded even higher heat capacities ($\sim 3.5 \text{ J(gK)}^{-1}$ at 76.8°C) than the GCAW, but when powdered in liquid nitrogen the heat capacities were lowered into the normal range ($\sim 0.8 \text{ J(gK)}^{-1}$ at 76.8°C). The measured heat capacity of the GCAW was reduced when placed in alumina powder. The anomalous behaviors are unexplained as of yet, but the effect is consistent and reproducible for both the same sample and among different samples.

An interesting phenomenon was found throughout this study dealing with heat capacity as a function of the location of the wire on the spool. As more measurements were performed, more wire was consumed on the spool of GCAW, which was accompanied by a spread in heat capacity (Figure 7). Since such a spread could result from inadequate sample contact with the

pan, experiments were carried out on a silicon standard with different contact areas, as the pan itself showed no effect. The contact of the silicon standard with the sample pan was manipulated in several heat cycles and there was not a substantial difference in heat capacity.

The spread in the heat capacity could result from structural differences along the length of wire due to the processing technique. In the glass – coated melt spinning method an ingot of the metal alloy is placed in a Pyrex® – type glass tube, which is then heated by an induction coil. The molten metal causes the glass to soften and a capillary is drawn, while rapidly cooled by a water jet. Many variables in this process could induce structural differences along the length of wire and it is clear that process control is vital to the manufacturing of consistent wire. At this time there is insufficient data to draw any conclusions regarding this possibility. Sato et al., however, observed that a variation in the magnetic properties of Fe – based amorphous alloys, including FeSiB compositions, along the ribbon length.⁴⁰ They verified that the disparities were due to variations of the roller surface temperature and ribbon thickness, which may also cause the heat capacity to differ along the length of the ribbon.

The influence of the glass cladding removal on the heat capacity of the wires was also studied. The measured heat capacity of both the CoFeSiB and FeSiB wire increased when the glass was removed, as seen in Figure 9. Pyrex® has a specific heat that is approximately two times that of a metal alloy so it would be expected that there would be a decrease in the heat capacity of the GCAW when the glass was removed.⁴¹ A decrease in fiber diameter, however, was previously found to increase the measured heat capacity and it is probable that the further increase in heat capacity of the GCAW is due to this effect.

In an attempt to do heat capacity measurements on samples with the same thermal history, a series of isothermal experiments was performed to determine a suitable annealing temperature (Figure 13). The first

temperature chosen was 544°C, which coincides with the approximate inflection point on the first exothermic peak of the FeSiB GCAW DSC curve. The crystallization peak obtained at 544°C corresponds to the second crystallization peak (Fe₃B) in the FeSiB GCAW DSC curve. Crystallization of Fe₃B at 544°C is immediate due to the high temperature and the reliance of this phase to nucleate on the already present $\alpha - (\text{Fe},\text{Si})$ phase, whose crystallization was instantaneous at this temperature. As the temperature was decreased to 534°C and lower, the evolution of another peak was observed, which correlates to the crystallization of $\alpha - (\text{Fe},\text{Si})$. This peak is visible at lower temperatures because more time is needed for the process to occur. Crystallization was found to occur at temperatures as low as 514°C, taking approximately 3 minutes to commence, suggesting that a practical annealing temperature may not exist. The amount of time necessary for any amount of relaxation to occur without crystallization would be far too long at a temperature well below the glass transition.

Although the glass transition has been found for several amorphous metal alloys, the T_g for all of the glass – covered amorphous metal wires and ribbon could not readily be determined using either traditional DSC and MDSC[®].^{20,42,43} The crystallization temperature coincides with this transition and the kinetics are far too rapid for it to be detected.

2. Thermogravimetric Analysis

A comparison of the Curie transitions for each of the glass – covered amorphous metal wires can be seen in Figure 14. The Curie transition of CoFeNiSiB (216°C) is more than 200°C lower than that of the base composition, FeSiB (436°C), while the Curie temperature of CoFeSiB occurs between these two at 322°C. Thus, the addition of both Co and Ni has a substantial influence on this transition. In all ferromagnetic materials, a magnetic interaction energy, or exchange energy exists, which is the amount of energy needed to cause the magnetic moments in the material to align.⁴⁴

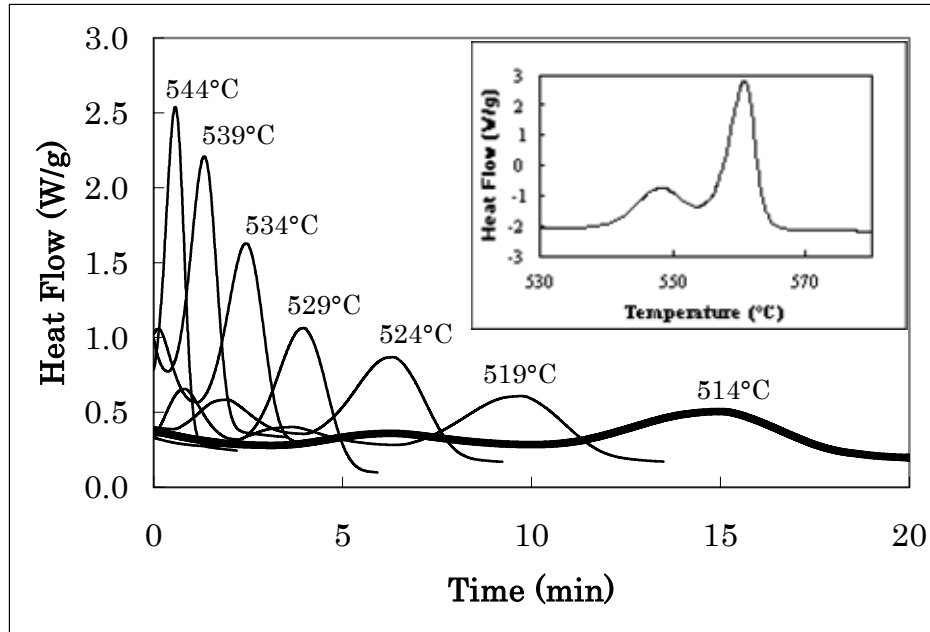


Figure 13. Isothermal study using the FeSiB GCAW at various annealing temperatures. An inset of the crystallization curve for FeSiB GCAW is provided for comparison.

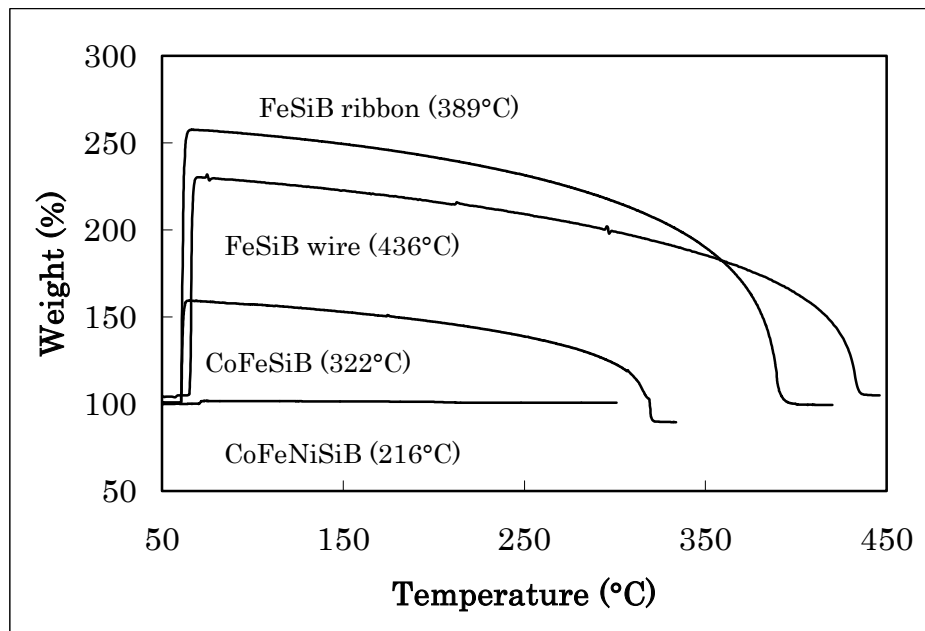


Figure 14. Comparison of the TGA curves for the FeSiB amorphous ribbon and the GCAW with the Curie temperatures stated. Note: All measurements were taken under the influence of a magnetic field.

As the temperature is increased, this energy is eventually overcome by the thermal energy at the Curie point, and the magnetic moments become randomized. The stronger the interaction energy is between the magnetic moments, the higher the Curie temperature. Therefore, as Co and Ni are added to FeSiB, the exchange energy is reduced, and the magnetic moments become unaligned at a lower temperature. The Curie temperature of the FeSiB ribbon (389°C) is somewhat lower than that of the wire, and as seen in Figure 12, it corresponds to the Curie temperature found by DSC. It is probable that the difference between the Curie temperature of the FeSiB GCAW and ribbon is due to the slight differences in iron and silicon content. Curie temperatures are structure – insensitive and should not be influenced by forming methods.⁴⁵ Luborsky et al. found a number of Curie temperatures in the Fe – Si – B system and determined that there is a rapid decrease in regions of increased iron content (75 – 85 %).²³ The replacement of boron by silicon resulted in slight increases in Curie temperatures. The Curie temperature of the FeSiB GCAW correlates very well to that found in the study by Luborsky. The composition of the FeSiB amorphous ribbon, however, was just outside the range studied and a comparison could not be made.

The FeSiB wire and ribbon appear to have the highest saturation magnetization since the weight had an apparent increase to ~220% when the magnet was placed under the furnace. CoFeSiB (~140%) and CoFeNiSiB (~102%) showed reduced effects. In order for a material to be ferromagnetic it must possess a net magnetic moment and as the magnitude of the magnetic moment is increased so does the saturation magnetization.^{44,46} Iron, for example, has four unpaired electrons and thus a net magnetic moment of $4\mu_B$ per atom, while cobalt has only $3\mu_B$ per atom, followed by nickel with $2\mu_B$ per atom. As Co and Ni are added to FeSiB, the magnetic moment and therefore saturation magnetization are decreased. Removing the glass from the wires does not affect Curie temperature, but it does increase the saturation

magnetization in the CoFeSiB and FeSiB GCAW, as the apparent weight percent increased above the previously listed values for each. It must be noted, however, that the total weight with the glass on includes the glass whereas the total weight with the glass removed includes only the metal. Thus, the weight percent change caused by the magnetization with the glass off will naturally be larger.

When the FeSiB ribbon was crystallized at 500°C (first crystallization peak), the Curie temperature of the metal shifted to 413°C, approximately 20°C higher than for the amorphous metal as seen in Figure 15. The crystalline metal also had a slightly higher saturation magnetization than the amorphous ribbon. Generally, the exchange energy in amorphous materials is weaker than in the corresponding crystalline structure, so both the Curie temperature and saturation magnetization would be lower.⁴⁶ As the ribbon was heated to 800°C, the wire passed through the first Curie transition and at the onset of the $\alpha - (\text{Fe}, \text{Si})$ crystallization there was a slight increase (~110 weight %) in the saturation magnetization. Upon the crystallization of Fe₃B, there was a significant increase in the saturation magnetization (~170 weight %) and the presence of a second Curie transition at approximately 698°C as seen in Figure 16. Efthimiadis et al. studied the crystallization of Fe₇₈Si₉B₁₃ and Fe₇₆Si₈B₁₆ amorphous ribbon through magnetic measurements and found this same result in the Fe₇₆Si₈B₁₆ ribbon.⁴⁷ The magnetic behavior of the Fe₇₈Si₉B₁₃ ribbon was slightly different since the two – stage crystallization mechanism took place over a much larger temperature range (~100°C). Two Curie transitions were also clearly visible in the FeSiB wire. The same trend was seen in the CoFeSiB wire, but the second Curie transition was barely detectable, as the saturation magnetization was very low. If the samples heated to 800°C, specifically the FeSiB wire and ribbon, are heated again, the Néel temperature is visible at 227°C, as seen in Figure 17. The Néel temperature is defined as the point at which an antiferromagnetic material returns to the paramagnetic state.⁴⁴ As

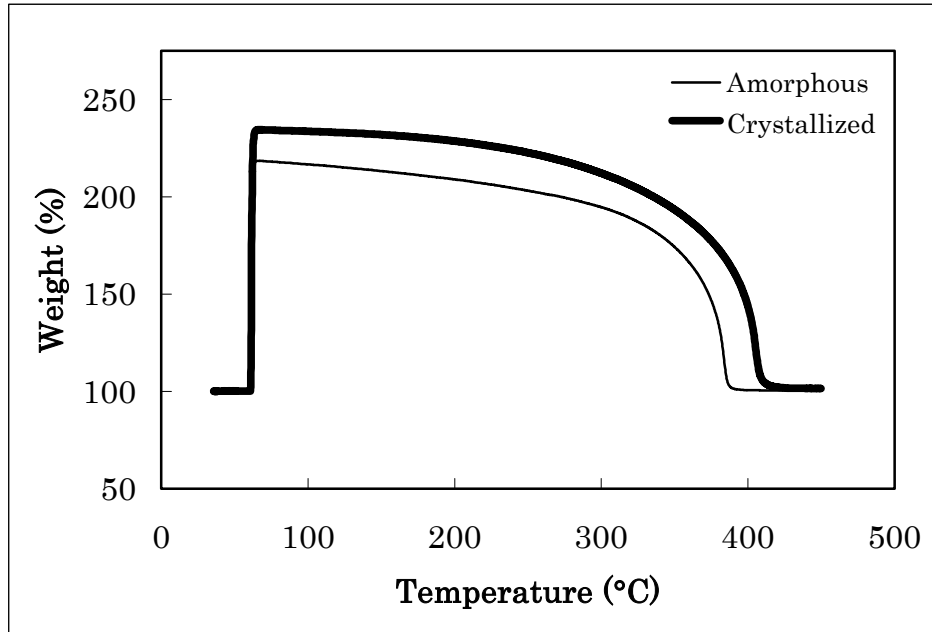


Figure 15. Comparison of the TGA curves for amorphous and crystallized FeSiB ribbon. Note: All measurements taken under the influence of a magnetic field.

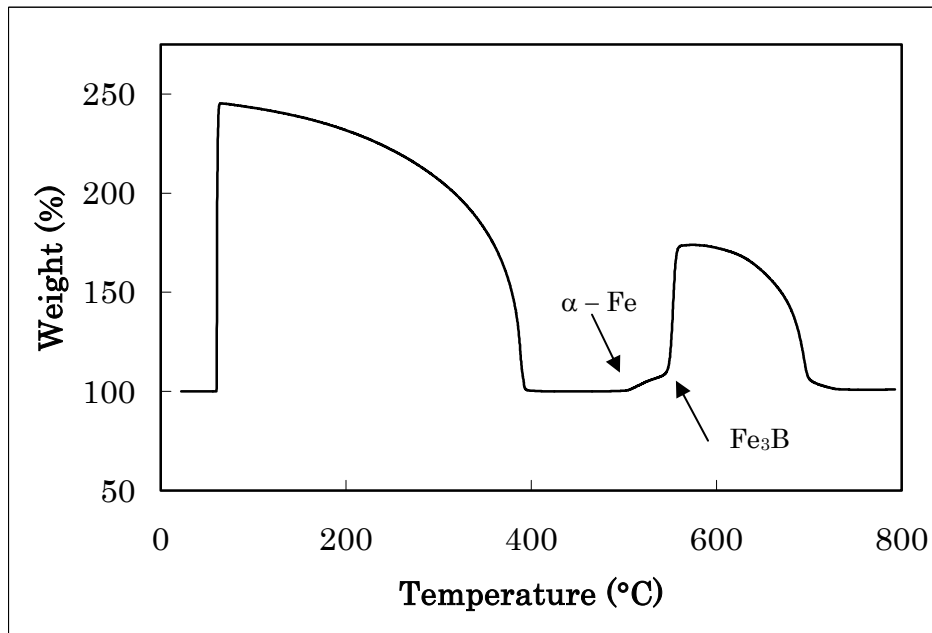


Figure 16. TGA curve of the FeSiB ribbon past the crystallization temperature denoting the onset crystallization temperatures of α -Fe and Fe₃B. Note: Measurement taken under the influence of a magnetic field.

these amorphous materials are heated to temperatures much greater than their crystallization a temperature, an irreversible magnetic reorientation occurs so that adjacent equal magnetic moments are antiparallel, leading to antiferromagnetic behavior. When heated past the Néel temperature, there is enough energy in the system to induce randomization of the magnetic moments and become paramagnetic.

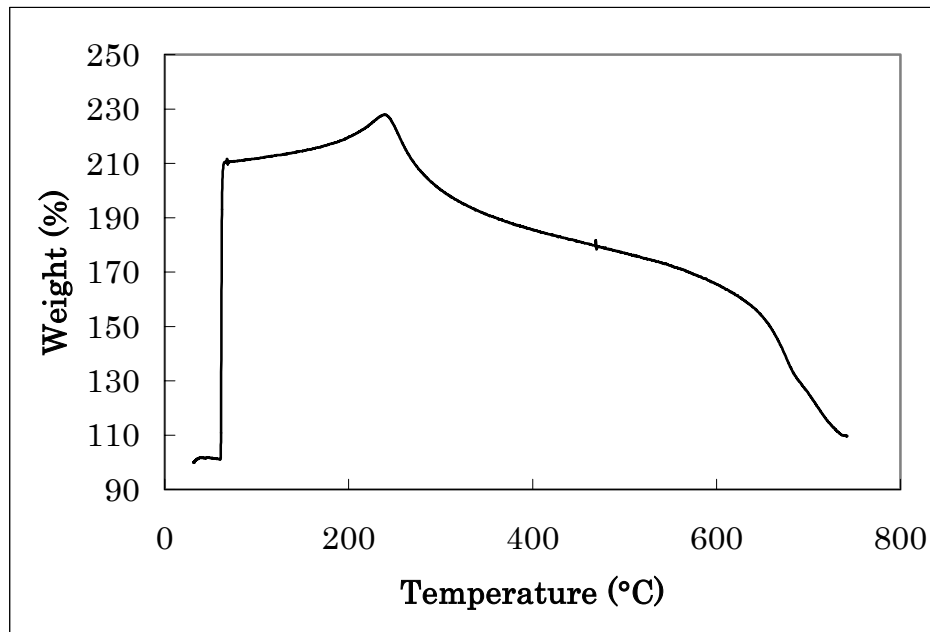


Figure 17. TGA curve of FeSiB GCAW showing the Néel temperature behavior. Note: Measurement taken under the influence of a magnetic field.

D. Conclusions

The addition of Co and Ni to the FeSiB wire has a strong influence on properties, such as crystallization temperature, heat capacity, Curie temperature, and saturation magnetization. The crystallization temperature increases as Co and Ni are added, since the presence of these atoms inhibits movement necessary for crystallization to occur. Both saturation magnetization and Curie temperature are decreased when these atoms are increased. Materials with higher exchange energies have higher Curie

temperatures and when Co and Ni are present, it takes less energy (lower temperature) to overcome the exchange energy and randomize the electronic spins. Saturation magnetization is simply influenced by the magnetic moments of the constituent atoms, and iron having the highest magnetic moment ($4\mu_B$ per atom) has the greatest magnetization. The magnetic moments of Co and Ni are lower, $3\mu_B$ per atom and $2\mu_B$ per atom, respectively, thus reducing the magnetization.

The presence of the glass coating apparently diminishes the magnetic behavior detected by the DSC and TGA and increases the heat capacities of the wire, but it does not have any influence on the crystallization temperatures. The amorphous ribbon has slightly lower crystallization temperatures than the FeSiB wire, which may be due to compositional differences, surface crystallization, or the presence of nuclei in the ribbon. Since the ribbon does not have the glass covering, the Curie temperature can be detected by the DSC and the saturation magnetization is higher than the wire. The Curie temperature, however, is lower in the ribbon than the wire due to slightly different compositions. When the ribbon and wires are crystallized there is an increase in the Curie temperature from an increase in the exchange energy. The GCAW show an anomalously high heat capacity, which is due to the wire aspect ratio, but is otherwise unexplained.

D. CONCLUSIONS

Modulated[®] DSC has been determined to be an efficient and consistent method for measuring heat capacities compared to the traditional DSC technique. Varying the instrumental parameters, which include heating rate, period, and amplitude, or the sample contact area did not have any unfavorable effects on the heat capacities found by MDSC[®] of a semiconductor grade silicon wafer. Generally, heat capacities measured by MDSC[®] were slightly higher than those determined by traditional DSC, the reason for which is unknown. A spread in the heat capacities measured by traditional DSC was observed, whereas there was little variation in the MDSC[®] heat capacities of the same FeSiB GCAW sample. There is no need to move the sample or open the DSC cell between each MDSC[®] measurement, so the experimental conditions are for the most part constant, which would lead to more consistent heat capacities. In traditional DSC, however, three thermal curves must be generated; consequently there is constant movement thus altering the sample environment.

Abnormally high heat capacities were measured for all three compositions of GCAW, reaching values as high as 22R at 326°C. Upon glass removal, heat capacities further increased. The same behavior was observed for typical borosilicate glass fiber, indicating that an anomaly exists in the heat capacity measurement of fibrous materials. As the fiber/wire diameter decreased, a corresponding increase in the heat capacity was detected. When the GCAW were placed in alumina, the heat capacity decreased, suggesting that a contact issue exists. At the present time the origin of the anomaly is otherwise unknown.

As Co and Ni are added to the amorphous alloy, the crystallization temperature is increased from 541°C for the FeSiB wire to 559°C for the CoFeNiSiB GCAW. The presence of these additional atoms hinders the movement necessary for crystallization to occur. Two consecutive

crystallization peaks were observed for the FeSiB GCAW and amorphous ribbon, which correspond to the crystallization of α – Fe and Fe₃B, respectively. It is probable that the difference in the crystallization temperatures of the FeSiB GCAW and amorphous ribbon is due to the slight compositional differences. Surface crystallization may also be a factor, but this is unlikely since there was no change in crystallization temperature after glass removal. There was evidence of the Curie temperature in the FeSiB amorphous ribbon DSC curve, while it was absent in the thermal curves of all three GCAW. The Curie temperature, however, was found in the FeSiB wire after glass removal, signifying that the glass – cladding acts as a barrier towards Curie temperature detection. Although the glass transition has been found in several other amorphous alloys, it was not determined for these alloy compositions, even using MDSC®. The crystallization temperature and glass transition were too close and the kinetics occurred far too quickly for it to be visible. The FeSiB GCAW had the highest relative heat capacity, followed by CoFeSiB, and then CoFeNiSiB. Differences in the contribution of the electronic heat capacity correspond to the decreased relative heat capacity as Co and Ni were added to the amorphous alloy.

Both Curie temperature and saturation magnetization decreased with additions of Co and Ni. The Curie temperature is influenced by the exchange energy between magnetic moments, which keeps the dipoles aligned. As the thermal energy becomes greater than the exchange energy, randomization occurs and material becomes paramagnetic. Therefore, the exchange energies are less in the CoFeSiB and CoFeNiSiB compositions, since the Curie transition occurs at a lower temperature. The Curie temperature of the crystalline alloy is slightly higher than the amorphous metal due to a higher exchange energy. Iron has the highest number of Bohr magnetons per atom (4 μ_B per atom, which causes the FeSiB GCAW and ribbon to have the highest saturation magnetizations. Additions of cobalt and nickel lower the saturation magnetization, as they have less Bohr magnetons than iron per

atom. If the GCAW or amorphous ribbon are heated to a temperature much greater than the crystallization temperature, two Curie transitions can be observed; one that corresponds to the amorphous metal and the second to the crystalline metal. When the same sample is heated again, the Néel transition is visible, which is the temperature that an antiferromagnetic material becomes paramagnetic.

E. FUTURE WORK

Since the origin of the anomalously high heat capacities of “fiber – type” could not be found in the extent of this study, it would be favorable to conduct additional experiments in an attempt to explain the phenomenon. The effect appeared to worsen as the fiber diameter was decreased, so the heat capacities of the same composition of glass fiber drawn to different diameters should be measured. Another experiment should involve cutting the same fiber into different consistent lengths to be placed in the sample pan to observe any changes in heat capacity. The use of different sample masses may also cause the heat capacity to deviate. Different masses of a silicon standard sample could be measured and then compared to the literature values.

In this series of experiments, the glass was always removed with liquid nitrogen. To determine the influence of the removal method on the properties of the GCAW, the glass should be removed by an acid etch and the properties should be measured again, specifically heat capacity. This would also be a good technique to use to determine the role of the glass covering; the glass could be etched for various amounts of time and then measured.

REFERENCES

1. M. Hagiwara, A. Inoue, and T. Masumoto, "Production of Amorphous Co-Si-B and Co-M-Si-B (M=Group IV - VIII Transition Metals) Wires by a Method Employing Melt Spinning into Rotating Water and Some Properties of the Wires," *Mater. Sci. Eng.*, **54** [2] 197-207 (1982).
2. F.B. Humphrey, "Applications of Amorphous Wire," *Mater. Sci. Eng. A*, **179-180** [Part 1] 66-71 (1994).
3. F.B. Humphrey, "Nearly 20 Years of Magnetic Amorphous Wire: An Overview," *J. Magn. Magn. Mater.*, **249** [1-2] 1-2 (2002).
4. P.T. Squire, D. Atkinson, M.R.J. Gibbs, and S. Atalay, "Amorphous Wires and Their Applications," *J. Magn. Magn. Mater.*, **132** [1-3] 10-21 (1994).
5. H. Chiriac, T.A. Ovari, G. Pop, and F. Barariu, "Effect of Glass Removal on the Magnetic Behavior of FeSiB Glass-Covered Wires," *IEEE Trans. Magn.*, **33** [1] 782-7 (1997).
6. H. Chiriac and T.-A. Ovari, "Magnetic Properties of Amorphous Glass-Covered Wires," *J. Magn. Magn. Mater.*, **249** [1-2] 46-54 (2002).
7. P. Marin and A. Hernando, "Applications of Amorphous and Nanocrystalline Magnetic Materials," *J. Magn. Magn. Mater.*, **215-216** 729-34 (2000).
8. H. Chiriac, "Preparation and Characterization of Glass Covered Magnetic Wires," *Mater. Sci. Eng. A*, **304-306** [1-2] 166-71 (2001).
9. H. Chiriac, C.S. Marinescu, T.A. Ovari, and M. Neagu, "Sensor Applications of Amorphous Glass-Covered Wires," *Sens. Actuators A*, **76** [1-3] 208-12 (1999).
10. "Modulated DSC (MDSC): How Does It Work?" (2004) TA Instruments. Accessed on: August, 2004. Available at <http://www.tainst.com/support/MDSC.pdf>
11. R.F. Speyer, *Thermal Analysis of Materials*; pp. 65-6. Marcel Dekker, New York, 1994.

12. H.H. Liebermann, J. Marti, R.J. Martis, and C.P. Wong, "The Effect of Microstructure on Properties and Behaviors of Annealed Fe₇₈B₁₃Si₉ Amorphous Alloy Ribbon," *Metall. Trans. A*, **20A** [1] 63-70 (1989).
13. C. Miguel, S. Kaloshkin, J. Gonzalez, and A. Zhukov, "Curie Temperature Behaviour on Annealing of Finemet Type Amorphous Alloys," *J. Non-Cryst. Solids*, **329** [1-3] 63-6 (2003).
14. V. Zhukova, S. Kaloshkin, A. Zhukov, and J. Gonzalez, "DSC Studies of Finemet-Type Glass-Coated Microwires," *J. Magn. Magn. Mater.*, **249** [1-2] 108-12 (2002).
15. M. Reading, D. Elliot, and V. Hill, "Some Aspects of the Theory and Practice of Modulated Differential Scanning Calorimetry," *Proc. Conf. North Am. Therm. Anal. Soc.*, **21** 145-50 (1992).
16. P.S. Gill, S.R. Sauerbrunn, and M. Reading, "Modulated Differential Scanning Calorimetry," *J. Therm. Anal.*, **40** [3] 931-9 (1993).
17. W.H. Press, B.P. Flannery, S.A. Teukolsky, and W.T. Vetterling, *Numerical Recipes: The Art of Scientific Computing*; pp. 386-90. Cambridge University Press, New York, 1986.
18. "Standard Test Method for Determining Specific Heat Capacity by Differential Scanning Calorimetry," ASTM Standard E1269-99. 2000 Annual Book of ASTM Standards, Vol. 14.02. American Society for Testing and Materials, West Conshohocken, PA, 2000.
19. F.F. Marzo, A.R. Pierna, and A. Altube, "Analysis of the Nanocrystallization of Finemet Type Alloy by Temperature-Modulated Differential Scanning Calorimetry," *J. Non-Cryst. Solids*, **287** [1-3] 349-54 (2001).
20. Y. Li, S.C. Ng, and Z.P. Lu, "Separation of Glass Transition and Crystallization in Metallic Glasses by Temperature-Modulated Differential Scanning Calorimetry," *Philos. Mag. Lett.*, **78** [3] 213-20 (1998).
21. "TA Instruments: Thermogravimetric Analyzers" (2004) TA Instruments. Accessed on: August, 2004. Available at <<http://www.tainst.com/support/newtgabrochure.pdf>>

22. "Standard Practice for Calibration of Temperature Scale for Thermogravimetry," ASTM Standard E1582-93. 2000 Annual Book of ASTM Standards, Vol. 14.01. American Society for Testing and Materials, West Conshohocken, PA, 2000.
23. F.E. Luborsky, J.J. Becker, J.L. Walter, and H.H. Liebermann, "Formation and Magnetic Properties of Fe-B-Si Amorphous Alloys," *IEEE Trans. Magn.*, **15** [3] 1146-9 (1979).
24. M.-S. Leu, J.S.C. Jang, C.-C. Lin, and W.-K. Wang, "The Effect of Composition on the Crystallization and Magnetic Transition of Fe-Si-B Amorphous Alloys," *Mater. Chem. Phys.*, **45** [3] 275-9 (1996).
25. G.F. Taylor, "A Method of Drawing Metallic Filaments and a Discussion of Their Properties and Uses," *Phys. Rev.*, **23** [5] 655-60 (1924).
26. V.N. Parkhachev, "Installation for Production of Glass Insulated Microwire Directly from Liquid Metal," U.S. Pat. 3256584, 1966.
27. H. Wiesner and J. Schneider, "Magnetic Properties of Amorphous Fe-P Alloys Containing Ga, Ge, and As," *Phys. Status Solidi A*, **26** [1] 71-5 (1974).
28. P. Duwez, "Structure and Properties of Alloys Rapidly Quenched from the Liquid State," *ASM Trans. Q.*, **60** 607-11 (1967).
29. T. Masumoto, A. Inoue, and M. Hagiwara, "Amorphous Metal Filaments and Process for Producing the Same," U.S. Pat. 4523626, 1985.
30. M. Hagiwara and A. Inoue, "Production Techniques of Alloy Wires by Rapid Solidification," in *Rapidly Solidified Alloys: Processes, Structures, Properties, and Applications*. Edited by H. H. Liebermann. Marcel Dekker, New York, 1993.
31. H. Chiriac, T.A. Ovari, G. Pop, and F. Barariu, "Amorphous Glass-Covered Magnetic Wires for Sensing Applications," *Sens. Actuators A*, **59** [1-3] 243-51 (1997).

32. P. Marin and A. Hernando, "Magnetic Microwires: Manufacture, Properties, and Applications," pp. 1-9 in *Encyclopedia of Materials: Science and Technology*. Edited by K. H. J. Buschow, R. W. Cahn, M. C. Fleming, B. Ilshner, E. J. Kramer, and S. Mahajan. Elsevier, Oxford, 2004.
33. H.H. Liebermann and C.D. Graham, Jr., "Production of Amorphous Alloy Ribbons and Effects of Apparatus Parameters on Ribbon Dimensions," *IEEE Trans. Magn.*, **12** [6] 921-3 (1976).
34. D.G. Archer, "Thermodynamic Properties of Synthetic Sapphire (α -Al₂O₃, Standard Reference Material 720 and the Effect of Temperature-Scale Differences on Thermodynamic Properties," *J. Phys. Chem. Ref. Data*, **22** [6] 1441-53 (1993).
35. *CRC Handbook of Chemistry and Physics*, 82nd ed.; p. 12.218. Edited by D.R. Lide. CRC Press, New York, 2001.
36. D.V. Ragone, *Thermodynamics of Materials*, Vol. 1; pp. 274 - 8. John Wiley & Sons, New York, 1995.
37. J.Y. Bang and R.Y. Lee, "Crystallization of the Metallic Glass Fe₇₈B₁₃Si₉," *J. Mater. Sci.*, **26** [18] 4961-5 (1991).
38. S. Elliot, *The Physics and Chemistry of Solids*; p. 300. John Wiley & Sons, New York, 1998.
39. L. Solymar and D. Walsh, *Lectures on the Electrical Properties of Materials*, 5th ed.; pp. 105-7. Oxford University Press, New York, 1993.
40. T. Sato, T. Ozawa, T. Yamada, and R. Matsumoto, "The Variation of Magnetic Properties of Fe-Based Amorphous Alloys Along the Ribbon Length," pp. 205-7 in *Materials Research Society Proceedings*, Vol. 8, *Rapidly Solidified Amorphous and Crystalline Alloys*. Edited by B. H. Kear, B. C. Giessen, and M. Cohen. North-Holland, New York, 1982.
41. W.D. Callister, Jr., *Materials Science and Engineering: An Introduction*, 5th ed.; pp. 812-4. John Wiley and Sons, New York, 2000.
42. J.L. Uriarte, A.R. Yavari, S. Surinach, P. Rizzi, G. Heunen, M. Baricco, M.D. Baro, and A. Kvick, "Properties of FeNiB-Based Metallic Glasses with Primary BCC and FCC Crystallization Products," *J. Magn. Magn. Mater.*, **254-255** 532-4 (2003).

43. Z.P. Lu, Y. Li, S.C. Ng, and Y.P. Feng, "Study of Glass Transition of Metallic Glasses by Temperature-Modulated Differential Scanning Calorimetry (MDSC)," *Thermochim. Acta*, **357-358** 65-9 (2000).
44. M. Barsoum, *Fundamentals of Ceramics*; pp. 559-602. McGraw Hill, New York, 1997.
45. C.W. Chen, *Magnetism and Metallurgy of Soft Magnetic Materials*; p. 98. Dover Publications, New York, 1986.
46. R.A. McCurrie, *Ferromagnetic Materials: Structure and Properties*; pp. 98-122. Academic Press, New York, 1994.
47. K.G. Efthimiadis, C.A. Achilleos, S.C. Chadjivasiliou, and I.A. Tsoukalas, "Study of the Crystallization of Amorphous $\text{Fe}_{78}\text{Si}_9\text{B}_{13}$ and $\text{Fe}_{76}\text{Si}_8\text{B}_{16}$ by Means of Magnetic Measurements," *Solid State Commun.*, **101** [7] 541-4 (1997).